

**Popular Summary:** Much of what we currently know about the large scale variability of and trends in the global sea ice cover has been based on data provided by satellite passive microwave sensors. While large changes in the sea ice cover have been observed during the satellite era, uncertainties in the trends have been difficult to assess because of the lack of adequate validation data. With the launched of the Advanced Microwave Scanning Radiometer in May 2002 on board the EOS-Aqua satellite (referred to as "AMSR-E"), however, ability to assess the accuracy of historical data has improved considerably because of much better resolution and hence accuracy in the former. This study shows that during the overlap period from June 2002 to 2006, highly consistent ice concentration maps can be derived from both AMSR-E and SSM/I data if the two data sets are inter-calibrated and the same algorithm is used to derive geophysical parameters. The ice extent estimates from SSM/I data, however, are consistently higher than those from AMSR-E while the ice area estimates are almost identical. This is shown to be caused by more precise definition of the ice edge provided by AMSR-E compared to that of SSM/I due to better resolution. Since the data record of AMSR-E is too short at less than 5 years, change studies using AMSR-E data can only be done if the latter are combined with historical satellite data. We show that this can be done successfully for ice area without any normalization of the data. It can also be done with ice extent through proper normalization of SSM/I and SMMR data. The estimates for trends in ice extent and ice area from the resulting data sets are shown to be consistent with those derived from historical data. The higher accuracy of the AMSR-E data, however, provides improved reliability in the data set and greater confidence in the trend values.

**Significant Findings:** With higher resolution and improved accuracy, AMSR-E data provide a good baseline for sea ice cover studies and can be used to validate geophysical parameters derived from historical data. Comparative studies of AMSR-E and SSM/I data during the 5 year period of overlap shows basically good consistency in the derived geophysical products. The most serious source of discrepancy is in the characterization of the ice edge and marginal ice zone in which AMSR-E clearly show improvements because of higher resolution. Thus SSM/I shows an ice edge location that is on the average about 6 to 12 km further away from the ice pack than AMSR-E data. Biases if uncorrected contribute to errors in the estimates of trends in extents by as much as 0.62%/decade in the Arctic and 0.26%/decade in the Antarctic. The biases in the trends of ice area are less with the error in the trend being at 0.30%/decade in the Arctic and 0.05%/decade in the Antarctic. Using time series data from SMMR, SSM/I and AMSR-E (starting June 2002) and after correcting for the aforementioned bias, the results of our regression analysis for period from November 1978 to December 2006 yielded trends in extent and area of sea ice in the Arctic region are  $-3.4 \pm 0.2$  and  $-4.0 \pm 0.2$  % per decade, respectively. The corresponding values for the Antarctic region are  $0.9 \pm 0.2$  and  $1.7 \pm 0.3$  % per decade. These trends are basically the same as those derived using SMMR and SSM/I data only, but with AMSR-E providing more accurate values for the last few years of the data set, the degree of confidence in the trend is higher with the latter included. With time, the data from AMSR-E and similar instruments will increase the reliability of the trend values.

**Title:** Trends in the Sea Ice Cover using Enhanced and Compatible AMSR-E, SSM/I and SMMR Data

**Authors:** Josefino C. Comiso, Cryospheric Sciences Branch, Code 614.1, NASA Goddard Space Flight Center, Greenbelt, MD 20771, email: Josefino.c.comiso@NASA.gov, and Fumihiko Nishio, Center for Environmental Remote Sensing, Chiba University 1-33 Yayoi-cho, Chiba City, Japan, email: fnishio@cr.chiba-u.ac.jp

**Journal:** JGR-Oceans - for the special section on "Large Scale Characteristics of the Sea Ice Cover from AMSR-E and other Satellite Sensors"

**Abstract:** Arguably, the most remarkable manifestation of change in the polar regions is the rapid decline (of about -10 %/decade) in the Arctic perennial ice cover. Changes in the global sea ice cover, however, are more modest, being slightly positive in the Southern Hemisphere and slightly negative in the Northern Hemisphere, the significance of which has not been adequately assessed because of unknown errors in the satellite historical data. We take advantage of the recent and more accurate AMSR-E data to evaluate the true seasonal and interannual variability of the sea ice cover, assess the accuracy of historical data, and determine the real trend. Consistently derived ice concentrations from AMSR-E, SSM/I, and SMMR data were analyzed and a slight bias is observed between AMSR-E and SSM/I data mainly because of differences in resolution. Analysis of the combine SMMR, SSM/I and AMSR-E data set, with the bias corrected, shows that the trends in extent and area of sea ice in the Arctic region is  $-3.4 \pm 0.2$  and  $-4.0 \pm 0.2$  % per decade, respectively, while the corresponding values for the Antarctic region is  $0.9 \pm 0.2$  and  $1.7 \pm 0.3$  % per decade. The higher resolution of the AMSR-E provides an improved determination of the location of the ice edge while the SSM/I data show an ice edge about 6 to 12 km further away from the ice pack. Although the current record of AMSR-E is less than 5 years, the data can be utilized in combination with historical data for more accurate determination of the variability and trends in the ice cover.

1  
2  
3  
4  
5  
6  
7  
8  
9  
10  
11  
12  
13  
14  
15  
16  
17  
18  
19  
20  
21  
22  
23  
24  
25  
26  
27  
28  
29  
30  
31

**Trends in the Sea Ice Cover using Enhanced and Compatible  
AMSR-E, SSM/I and SMMR Data**

Josefino C. Comiso  
Cryospheric Sciences Branch, Code 614.1, NASA Goddard Space Flight Center  
Greenbelt, MD 20771, email: Josefino.c.comiso@NASA.gov

Fumihiko Nishio  
Center for Environmental Remote Sensing, Chiba University  
1-33 Yayoi-cho, Chiba City, Japan, email: fnishio@cr.chiba-u.ac.jp

Submitted to JGR-Oceans  
Special Section on "Large Scale Characteristics of the Sea Ice Cover from AMSR-E and other  
Satellite Sensors"

Running Title: Trends in the Sea Ice Cover from Space  
Keywords: Sea ice, Arctic and Antarctic, Climate Change, Satellite Remote Sensing

32

33

### Abstract

34

35

36

37

38

39

40

41

42

43

44

45

46

47

48

49

50

51

52

### 1. Introduction

53

54

55

56

57

58

59

60

61

62

63

Arguably, the most remarkable manifestation of change in the polar regions is the rapid decline (of about -10 %/decade) in the Arctic perennial ice cover. Changes in the global sea ice cover, however, are more modest, being slightly positive in the Southern Hemisphere and slightly negative in the Northern Hemisphere, the significance of which has not been adequately assessed because of unknown errors in the satellite historical data. We take advantage of the recent and more accurate AMSR-E data to evaluate the true seasonal and interannual variability of the sea ice cover, assess the accuracy of historical data, and determine the real trend. Consistently derived ice concentrations from AMSR-E, SSM/I, and SMMR data were analyzed and a slight bias is observed between AMSR-E and SSM/I data mainly because of differences in resolution. Analysis of the combine SMMR, SSM/I and AMSR-E data set, with the bias corrected, shows that the trends in extent and area of sea ice in the Arctic region is  $-3.4 \pm 0.2$  and  $-4.0 \pm 0.2$  % per decade, respectively, while the corresponding values for the Antarctic region is  $0.9 \pm 0.2$  and  $1.7 \pm 0.3$  % per decade. The higher resolution of the AMSR-E provides an improved determination of the location of the ice edge while the SSM/I data show an ice edge about 6 to 12 km further away from the ice pack. Although the current record of AMSR-E is less than 5 years, the data can be utilized in combination with historical data for more accurate determination of the variability and trends in the ice cover.

Much of what we currently know about the large scale variability of the global sea ice cover has been based on data provided by satellite passive microwave sensors (Parkinson et al., 1999; Bjorgo et al., 1999; Zwally, 2002). This capability for studying the sea ice cover has recently been improved considerably with the launched of the Advanced Microwave Scanning Radiometer in May 2002 on board the EOS-Aqua satellite (referred to as "AMSR-E") and in December 2002 on board Midori-2 (called "AMSR"). In this paper, we will use results primarily from AMSR-E which is the only sensor of the two that is currently providing data because of the unexpected power failure in the Midori-2 satellite after 9 months of operation. The improvements of AMSR-E over the Special Scanning Microwave Imager (SSM/I), which has been the primary source of data since July 1987, include higher resolution at all frequencies, wider spectral range, and less radiometer noise. In particular, AMSR-E has integrated field-of-

64 views of 26.2 by 16.5 km and 13.7 by 10.3 km with its 18.7 and 36.5 GHz channels for mean  
65 resolutions of 21 and 12 km, respectively. On the other hand, SSM/I has integrated field-of-  
66 views of 70 by 45 km and 38 by 30 km with its 19.35 and 37.0 GHz channels for mean  
67 resolutions of 56 and 33.8 km, respectively. AMSR-E scans conically with a swath width of  
68 1450 km at an incidence angle of  $55^\circ$  while SSM/I scans with a swath width of 1390 km at an  
69 incidence angle of  $53.1^\circ$ . The wider swath for AMSR has enabled almost complete coverage near  
70 the poles where data are usually missing due to satellite inclination. Also, AMSR-E has twelve  
71 channels from 6 GHz to 89 GHz, while SSM/I has only 7 channels from 19 GHz to 85 GHz. The  
72 lower frequency channels (6.9 and 10.65 GHz) of AMSR-E provide the ability to retrieve Sea  
73 Surface Temperature (SST) and Surface Ice Temperature (SIT) that are useful not only as climate  
74 data sets but also in removing ambiguities in the retrievals due to atmospheric and surface  
75 temperature effects. Furthermore, the higher resolution minimizes the uncertainties associated  
76 with the use of mixing algorithms to retrieve geophysical sea ice parameters.

77         The polar regions are expected to provide early signals of a climate change primarily  
78 because of the so called "ice-albedo feedback" which is associated with the high reflectivity of ice  
79 and snow covered areas compared to ice free areas. Recent reports have indeed shown that the  
80 perennial ice cover in the Arctic has been declining at a rapid rate of about 10 % per decade  
81 (Comiso, 2002; Stroeve et al., 2004, Comiso, 2006). While this has led to speculations of an ice  
82 free Arctic in summer within this century, hemispherical changes including those from seasons  
83 other than summer have been more modest at about 2 to 3% per decade (Bjorgo et al., 1997;  
84 Parkinson et al., 1999; Serreze, 2000). Moreover, in the Antarctic, the trend is also modest but in  
85 the opposite direction (Cavalieri et al., 1997; Zwally et al., 2002). The significance of estimates  
86 in the trends, have not been fully evaluated because of unknown uncertainties in the parameters  
87 derived from historical satellite data. A key problem is that data from a number of different  
88 sensors have to be assembled together to make up the historical time series of satellite data we  
89 currently have. There are also mismatches in calibration and resolution and there are no  
90 measurements that can be used to assess the true large scale characteristics of the sea ice cover  
91 and evaluate the accuracy of existing ice data.

92         The launch of AMSR-E is thus timely in this regard in that the data provide the much  
93 needed baseline for evaluating the historical record of satellite ice data including the validity of  
94 aforementioned trends. Although the time series of AMSR-E data is still short it can also be used  
95 in conjunction with historical data to obtain even more accurate trend values. Analysis of

96 AMSR-E data benefits from the availability of the Moderate Resolution Imaging  
97 Spectroradiometer (MODIS) on board the Aqua satellite which provides concurrent observations  
98 of the same surface as AMSR-E at a much higher resolution (250 m) during clear skies  
99 conditions. Preliminary studies have shown that ice characterization from AMSR-E agrees  
100 favorably with those MODIS data in the visible channels obtained during clear sky conditions  
101 (e.g., Comiso, 2004).

102

## 103 2. Consistent Retrieval of Sea Ice Concentrations

104 The spatial distributions of sea ice in the two hemispheres are quite different in that sea  
105 ice is surrounded by continental land masses in the Northern Hemisphere while in the Southern  
106 Hemisphere, it is sea ice that surrounds a land mass, which in this case is continental Antarctica  
107 (Figure 1). In the winter, the Arctic basin is basically covered by consolidated ice that is more  
108 confined, thicker and colder than those in the Antarctic. In the Arctic, a large fraction of the ice  
109 floes survives the summer melt and can be as old as 7 years (Colony and Thorndike, 1985), while  
110 in the Antarctic, it is rarely the case that an ice floe is older than 2 years, the reason being that the  
111 ice that survives the summer melt in the region usually gets flushed out of the original location  
112 and to the warmer waters by strong ocean currents (e.g., Weddell gyre) during autumn and  
113 winter. Also, the impact of divergence on Antarctic sea ice is stronger than in the Arctic because  
114 of the lack of an outer boundary in the former, causing more and larger leads and basically more  
115 new ice than in the former.

116 Sea ice is an inhomogeneous material consisting of ice, brine, air pockets, and other  
117 impurities, the relative percentages of which are different depending on formation conditions and  
118 history of the ice (Weeks and Ackley, 1986; Tucker et al., 1992; Eicken, 1991). We now know  
119 that these inhomogenities affect the dielectric properties of sea ice in the two regions and hence  
120 the emissivity or radiative characteristics (Vant et al., 1974; Grenfell, 1992). Hemispherical  
121 differences in environmental conditions thus make the radiative signatures of sea ice in the Arctic  
122 generally different from those in the Antarctic. This leads to differences in the brightness  
123 temperatures as measured by passive microwave sensors, especially for consolidated ice, making  
124 it necessary to use different input data for the sea ice algorithms used to retrieve sea ice  
125 parameters in the two hemispheres (Comiso et al., 2003a; Comiso, 2004).

126 Among the most basic geophysical cryospheric parameters that are derived from passive  
127 microwave data is sea ice concentration. Sea ice concentration,  $C_I$ , has been defined as the

128 percentage fraction of sea ice within the field of view of the sensor. Such percentage has been  
129 calculated using a linear mixing equation (Zwally et al., 1983) given by

130

$$131 \quad T_B = T_I C_I + T_O (1 - C_I) \quad (1)$$

132

133 where  $T_B$  is the observed brightness temperature while  $T_I$  and  $T_O$  are the brightness temperature  
134 of sea ice and open water, respectively, in the region of observation. The sea ice algorithms are  
135 formulated with a goal of estimating  $T_I$  and  $T_O$  within the satellite footprint as accurately as  
136 possible. In the Rayleigh-Jeans' approximation, the brightness temperature of a surface is equal  
137 to its effective emissivity multiplied by the physical temperature of the emitting surface. The  
138 equation (1) suggests that data from only one channel is required but ability to obtain the  
139 appropriate  $T_I$  and  $T_O$  values would be limited because of known spatial and temporal variability  
140 of emissivity and temperature within the ice pack (Comiso, 1983; Parkinson et al., 1987; Comiso,  
141 1995). The advent of multichannel systems, such as SMMR, allowed the development of  
142 algorithms that circumvents this problem (Cavalieri et al., 1984; Svensen et al., 1984; Swift et al.,  
143 1986; Comiso, 1986). Such algorithms have been further refined to take advantage of the added  
144 capabilities of the AMSR-E sensor (Markus and Cavalieri, 2000; Comiso et al., 2003). This  
145 study makes use of the Bootstrap algorithm, that utilizes the 19 and 37 GHz channels at vertical  
146 polarization and the 37 GHz channels at horizontal polarization for both hemispheres, as  
147 described in Comiso(2004).

148 Change studies, especially in relation to climate, require as long historical record as  
149 possible. Unfortunately, current record on global sea ice cover data has not been that long since  
150 such data did not exist until the advent of the satellite era. The era started with the Nimbus-  
151 5/Electrically Scanning Microwave Radiometer (ESMR) which was launched in December 1972  
152 and was the first microwave imaging (or scanning) system. The sensor is a one-channel system  
153 with a peak frequency of about 19 GHz and acquires data at variable incidence angles (since  
154 scanning is done cross-track). The more current sensors like SMMR, SSM/I and AMSR-E are  
155 conically scanning sensors that acquire data at fixed angles thereby making the latter easier to  
156 interpret and to be used in the retrieval of geophysical parameters. The ice concentrations  
157 derived from the ESMR sensor are thus not as accurate as those from the other sensors mainly  
158 because single channel data do not provide the means to resolve ambiguities associated with the  
159 presence of many ice types that have different emissivities. Furthermore, the ESMR data set has

160 lots of gaps (sometimes several months for each year) because of hardware related problems.  
161 While ESMR provided some useful sea ice data during the 1973 to 1976 period, trend studies of  
162 the sea ice cover usually starts with the SMMR data and covering the period from November  
163 1978 to the present for optimum accuracy. But even with this restriction, putting together a data  
164 set using SMMR, SSM/I and AMSR-E is not trivial because of different attributes and  
165 characteristics of the different sensors. As will be discussed, mismatches in the locations of the  
166 ice edges can occur because of different resolutions and other factors. There can also be  
167 mismatches in ice concentration from different sensors on account of slightly different peak  
168 frequencies, different incident angles and different calibration for the different sensors.

169         The initial step for this study is to create a time series of sea ice data from the different  
170 sensors that are as consistent as possible. In particular, we made the brightness temperatures  
171 (TBs) for the different sets of channels used to generate the ice concentration maps to match to  
172 each other as closely as possible. This in part minimizes effects of inconsistent calibration,  
173 incident angle, and peak frequency. This was done by first making SSM/I TBs to be consistent  
174 with those of AMSR-E TBs for each set of channels by normalizing the values of the former  
175 using parameters derived from linear regression of data from the two sensors during overlap  
176 periods. This was followed by making data from the different SSM/I sensors consistent and after  
177 that by getting the SMMR TBs consistent with SSM/I TBs. The next step is to use same sea ice  
178 concentration algorithm (i.e., the Bootstrap Algorithm as indicate above) for data from all  
179 sensors. Although it is the same formulation, the Bootstrap Algorithm will be called ABA when  
180 applied to AMSR-E data and SBA when applied to SSM/I data. Finally, the same techniques are  
181 used for the land mask, ocean mask, and land/ocean boundary masks as described in Comiso  
182 (2004) when generating the ice concentration maps.

183         To illustrate how well we succeeded with the aforementioned strategy, ice concentration  
184 maps from AMSR-E and SSM/I on 15 February 2003 in the Northern Hemisphere and on 15  
185 September 2003 in the Southern Hemisphere are shown in Figure 2. In general, the technique  
186 appeared to have worked very well with the resulting daily ice concentration maps from different  
187 sensors showing very good agreement during overlapping periods. There are subtle differences  
188 especially near the ice margins associated with differences in resolution and antenna patterns of  
189 the different sensors but ice concentration values in practically all regions are virtually identical.

190



191 The good agreement in ice concentration is encouraging since it means that the same features of  
192 the ice cover are reproduced by the different sensors. The minor differences, which are mainly  
193 confined near the marginal ice zones, are inevitable because of innate differences in resolution,  
194 the peak frequencies for the radiometer channels used in the algorithm, the incident angle and the  
195 antenna side lobes. To gain insight into these differences, we first examine the procedure for  
196 masking open ocean areas which is basically done by setting a threshold below which the data is  
197 considered as open ocean. The large contrast of the passive microwave signature of sea ice and  
198 open water at some of the channels has enabled estimates of the ice concentration at almost all  
199 values except at some low ice concentration values where the signature of open water and ice  
200 covered surfaces are virtually identical. Moreover, areas in the open ocean that are under the  
201 influence of abnormal weather conditions can have signatures similar to those of ice covered  
202 ocean. The use of a combination of 19, 22, and 37 GHz channels for the sensors, however,  
203 allows for effective discrimination of open ocean data under unusual conditions as illustrated in  
204 the scatter plots in Figure 3. In figures 3a and 3b, we show scatter plot of TB(19,V) versus the  
205 difference  $TB(22,V) - TB(19,V)$  using SSM/I and AMSR data, respectively, while in figures 3c  
206 and 3d, we show the corresponding plots but of TB(19,V) versus TB(37,V). The blue data points  
207 in the scatter plot along OW actually represent data from the open ocean at all weather conditions  
208 while the black data points are those from ice covered ocean. Open water within the pack is  
209 usually relatively calm and provides the lowest emissivity of data points along OW and is  
210 therefore represented in the algorithm as a data point close to the label O. In the open ocean the  
211 surface gets disrupted occasionally by strong winds and bad weather causing big waves and foam,  
212 causing the signature to move to higher values and towards W in the scatter plot, depending on  
213 the strength of the disruption. In the algorithm, data points along OW are masked to represent  
214 open water only with the red line, representing approximately 10% ice concentration used as the  
215 threshold as described in Comiso et al. (2003). To obtain consistent ice extent and ice area from  
216 SSM/I and AMSR-E data, it is thus important to have the same threshold for both sensors. The  
217 set of data points between O and W which are considered as open water areas and should be  
218 separated from the ice covered surfaces with 10% ice concentration and above in the same way.

219 The higher resolution of AMSR provides a better definition of the marginal ice zone and a  
220 more precise location of the ice edge as previously indicated by Worby and Comiso (2000). This  
221 is clearly illustrated in the plots of brightness temperatures at different frequencies across the  
222 marginal ice zone (i.e., 35° W longitude) in the Antarctic for both AMSR and SSM/I (Figure 4).

223 The plots show that the brightness temperatures are relatively low and uniform in the open water  
224 (left side) and gradually increase over the marginal ice zone and reached their highest values over  
225 the consolidated ice region. Over the marginal ice zone that includes the ice edge, the changes in  
226 TBs are coherent and consistent at all AMSR-E frequencies. The TBs are not so consistent for  
227 the different SSM/I channels (not shown). The corresponding plots for ice concentration, as  
228 shown in Figure 4c, indicate that AMSR-E provides a more defined ice edge than SSM/I with the  
229 latter further away from the pack by about 12 km. Such discrepancy makes it almost impossible  
230 to get a perfect match in the estimates of ice extent using data from the two sensors as will be  
231 discussed later. Similar plots for ice concentration in the Barents Seas in the Northern  
232 Hemisphere along the 35 °E and 45 °E longitudes (Figures 5a and 5b) show basically the same  
233 effect but sometimes, the difference can be more modest. It is apparent that a bias exists, with the  
234 SSM/I data showing a location of the ice edge that is further away from the pack than the AMSR-  
235 E data. This phenomenon is associated with differences in resolution and side lobes of the  
236 antenna. The coarser the resolution is, the more the ice covered areas overlap with the open  
237 ocean. The effect of the antenna sidelobe is to cause a smearing at the ice edge since higher  
238 brightness temperature is observed as the satellite crosses the ice edge from the pack to the open  
239 ocean than vice versa. Such smearing is more pronounced with the SSM/I than the AMSR-E data  
240 which has a narrower field-of-view (and higher resolution) than the former.

241

### 242 **3. Comparison of Sea Ice Extents, Area and Ice Concentration during Overlap Period**

243 The ice parameters derived from satellite ice concentration data that are most relevant to  
244 climate change studies are sea ice extent and ice area. Ice extent is defined here as the integrated  
245 sum of the areas of data elements (pixels) with at least 15% ice concentration while ice area is the  
246 integrated sum of the products of the area of each pixel and the corresponding ice concentration.  
247 Ice extent provides information about how far north the ice goes in winter and how far south it  
248 retreats towards the continent in the summer while the ice area provides the means to assess the  
249 total area actually covered by sea ice, and also the total volume and therefore mass of the ice  
250 cover, given the average thickness. In the previous section we discussed the technique we used  
251 for obtaining consistent ice concentrations from the various sensors. We now show how  
252 consistently we can get the ice extent and ice area from these sensors as well as average ice  
253 concentrations during periods of overlap. Figures 7a-7f show distributions of daily average ice  
254 extent, ice area and ice concentration over an entire annual cycle using AMSR-E and SSM/I data

255 in 2005 for both Northern and Southern Hemispheres. The plots in Figures 7a and 7b show that  
256 the extents derived from SSM/I data (in blue) are consistently higher than those from AMSR-E  
257 data (in red) with the difference in winter relatively smaller than those in the summer period. The  
258 plots in Figures 7c and 7d show that the ice areas derived from SSM/I are still higher but much  
259 more consistent with those derived from AMSR-E data. These results suggest that the mismatch in  
260 resolution affects estimates of the extent more than the ice area with the coarser resolution system  
261 (i.e., SSM/I) providing the higher extent because of smearing effect as described earlier. The  
262 average ice concentrations from AMSR-E (Figures 7e and 7f) are also shown to be consistently  
263 higher by about 1 to 2% than that of SSM/I. This in part made the ice area from the two sensors  
264 more compatible. The main reason for the difference in extents from the two sensors is that there  
265 are more data elements with ice for SSM/I than AMSR-E, mainly because the ice edges in the  
266 former extends further beyond the MIZ than the latter, as discussed earlier. These additional data  
267 elements have low concentration values the inclusion of which causes the average ice  
268 concentration to be lower. The additional low ice concentration data also makes the average ice  
269 concentration lower for SSM/I than AMSR. The discrepancy is not so apparent with the ice area  
270 because the ice concentrations maps (see Figure 2, for example) basically match each other and  
271 the contribution of low concentration pixels at the ice edge is not as significant for ice area as  
272 with the ice extent estimates.

273         Similar comparative analysis of ice extents, ice area and ice concentration using data from  
274 two SSM/I sensors (i.e., F11 and F13) during the period of overlap from May to September 1995  
275 is presented in Figure 8. The plots show very good agreement of data from the two sensors. This  
276 is not a surprise since the two sensors have virtually the same attributes. Slight differences in ice  
277 concentration estimates occur (e.g., 20 July 1995) but this may be associated with radiometer  
278 noise. It should be noted, that the good agreement was obtained after the two sensors were  
279 intercalibrated and the TBs were made consistent. Although the resolutions of F11 and F13 are  
280 expected to be the same, consistency in the derived ICs is needed to get consistency in the extent  
281 and area.

282         During the overlap of SSM/I and SMMR data in mid July to mid-August in 1987 the  
283 extents and areas are also in relatively good agreement (Figure 9) during this summer period in  
284 the Arctic and the winter period in the Antarctic. It is interesting to note that the agreement was  
285 better during August than in July in the Northern Hemisphere but the opposite is true in the  
286 Southern Hemisphere. Also, the SSM/I values tend to be higher than those of SMMR in the

287 Northern Hemisphere in July while the reverse is true in the Southern Hemisphere in August.  
288 Furthermore, the differences in the average ice concentrations are larger in the Northern  
289 Hemisphere than in the Southern Hemisphere and in July, SSM/I values are higher than those of  
290 SMMR while the opposite is true in July of the Southern Hemisphere. Because of these  
291 inconsistencies, it is not easy to establish whether there is a bias or not, especially since the  
292 overlap period is quite short.

293 Degradation in the quality of the SMMR data was occurring during this period and it is  
294 likely that the SMMR observations were not as accurate as those of SSM/I. An overlap of at least  
295 one annual cycle would have been desirable if only to establish that the seasonal differences are  
296 similar to those shown in Figure 8. In the time series that requires monthly averages, SMMR  
297 data were used to generate monthly data for July 1987 while SSM/I data were used for the August  
298 monthly. This procedure appears good for the Antarctic data since there is good consistency of  
299 the two sensors in this region in July but such advantage is not apparent the Northern  
300 Hemisphere.

301 It is encouraging that the agreement between AMSR-E and SSM/I ice extents and area data  
302 is as good as indicated in the plots despite the vast differences in resolution. The use of ice  
303 concentration is expected to take care of the resolution problem but not completely especially in  
304 the estimates of ice extent. As indicated earlier, the data with lower resolution will find the ice  
305 edge further away from the pack than the one with higher resolution. Although the same  
306 algorithm is applied on the two data sets, the fields of view and side lobes of the two sensors are  
307 different and hence the observed radiances from the two sensors cannot be identical even if the  
308 calibration of each is perfect. Also, the location of the ice margins as observed by the two  
309 sensors are not expected to be same. One key reason for this is the differences in revisit time of  
310 the two sensors: one (SSM/I) crossing the equatorial line at about 10 am while the other (AMSR-  
311 E) at about 1 pm. Since the ice cover is dynamic and the ice edge can easily be altered by winds,  
312 the ice edge location can be significantly changed within the three hour difference.

313 It is apparent that errors (or biases) in ice extent has to be considered when combining  
314 data from different sensors with different resolutions. This already assumes that the ice  
315 concentrations are derived in a similar fashion and the masking for open water, land and  
316 ice/ocean boundaries are similar if not identical. There are also mismatches in the estimates for  
317 ice area but they are basically small and negligible.

318

## 319 4.0 Monthly Changes and Interannual Trends in the Sea Ice Extents and Areas

320

### 321 4.1 The Northern Hemisphere

322 The time series of monthly sea ice extents and areas in the Northern Hemisphere from  
323 1978 to the present, as presented in Figure 10, provides the means to evaluate how the ice cover  
324 in the entire Northern Hemisphere has been changing during the satellite era. The variabilities in  
325 both extent and area are similar and are dominated by a very large seasonality of the ice cover in  
326 the region as has been cited previously (e.g., Parkinson et al., 1987). The ice minimum usually  
327 occurs in September while the ice maximum occurs either in February or March. The time series  
328 shows data from the different sensors in different colors and show basically a smooth transition  
329 from one sensor to the other. Although there is overlap of SMMR and SSM/I data for about a  
330 month from mid-July to mid-August 1987, the plot shows averages from SMMR for July 1987  
331 and that for SSM/I for August 1987. The only overlap presented is that of SSM/I and AMSR-E  
332 which started in June 2002 and continued through 2006. During overlap period, SSM/I extent  
333 and area are slightly higher than those of AMSR-E as expected from previous discussions.

334 The monthly data show large interannual variability in the peak values, the amplitude and  
335 also the minimum values for both extent and area. The patterns are also not so predictable with  
336 high values in winter not necessarily leading to high values in the summer (e.g., 1974 and 1990).  
337 To assess how the length of the growth period has changed over time, the dates of ice minimum  
338 and maximum were identified for each year. The length of growth in our case is defined as the  
339 time period between the date of ice minimum in one year to the date of ice maximum the  
340 following year and for the period 1979 to 2005 and the results gave an average length of 179 days  
341 and a declining trend of about -2.5 days per decade. The minimum and maximum dates changes  
342 with time but it appears that the difference changes only by a few days and the length of growth  
343 had so far been basically stable. It is also apparent that the peak values have been going down  
344 since 2002 while the minimum values have been abnormally low during the same years.

345 To assess interannual trends in the ice cover, we use monthly anomalies as has been done  
346 previously (Parkinson et al., 1999; Zwally et al., 2002) in order to minimize the effect of the large  
347 seasonal variations. These anomalies were obtained by subtracting the monthly climatological  
348 averages from each monthly average. The climatology for each month is the average of all data  
349 for this month from November 1978 to December 2006. The monthly anomalies for the ice  
350 extents in the Northern Hemisphere are presented as three different combinations of combining

351 the data in Figure 11, namely: (a) SMMR and SSM/I extents only, (b) SMMR, SSM/I and  
352 AMSR-E extents with SSM/I data ending where AMSR-E data starts, and (c) normalized SMMR  
353 and SSM/I and original AMSR-E extents. Normalization parameters for the last case are derived  
354 from data during SSM/I and AMSR-E overlap and are meant to get the two data sets consistent  
355 during the period. The first case provides the data that is currently being utilized for trend studies  
356 while the second case make use of AMSR-E data instead of SSM/I when appropriate. The trend  
357 values for SMMR and SSM/I data only is  $-3.39 \pm 0.18$  % per decade while that for SMMR,  
358 SSM/I and AMSR-E data is  $-3.99 \pm 0.20$  % per decade. There is a difference of  $-0.60$  % per  
359 decade in the trends but this is likely associated with the bias as described earlier, due in part to  
360 the difference in resolution between AMSR-E and SSM/I. When the bias is removed through  
361 aforementioned renormalization, the trend for a combined SMMR, SSM/I and AMSR-E data is -  
362 3.37 which is consistent with that for SSM/I and SMMR data only. Taking advantage of the  
363 overlap thus enables the AMSR-E data to be utilized in trend analysis. Since the latter is more  
364 accurate, the net error in the trend analysis is going to be less and the importance of AMSR-E  
365 data in trend studies will increase with time.

366 The range of variability in the anomalies is about  $1 \times 10^6$  km<sup>2</sup> while that for seasonal ice,  
367 as revealed by the monthly averages, is about to  $8 \times 10^6$  km<sup>2</sup>. It is also apparent that the  
368 variability is significantly less for the period 1996 to 2006. This is intriguing since the slope of  
369 the data during the latter period appears different from those of the earlier period. Linear  
370 regression using only data from 1996 to 2006 yields a trend of more than  $-8\%$  per decade, which  
371 is more than twice the trend from 1978 to 2006. During the last ten years, many unusual events  
372 happened in the Arctic. First, there was a record high ice free region in the Beaufort Sea in 1998  
373 (Comiso et al., 2003) which was then the warmest year on record globally over a century (or  
374 since temperature sensors started to be used). There was also a record low perennial ice cover in  
375 2002 which at the same time became the warmest year on record. The perennial ice cover was a  
376 record low again in 2005 which also became the warmest year on record. The intervening  
377 periods were low ice years as well including that of 2006. It is possible that the values before  
378 1996 are representative of the natural variability of sea ice cover in the Arctic but the changes  
379 after that may not be part of the natural variability as previously suggested (Overland, 2005). The  
380 Arctic ocean surface is expected to warm up as the perennial ice continues to retreat on account  
381 of the so called "ice-albedo feedback," and a warmer ocean would delay the onset of ice growth  
382 in the autumn and cause an earlier melt onset, thereby causing a shorter ice season and hence

383 thinner and less extensive ice cover. With additional warming expected from increasing  
384 greenhouse gases in the atmosphere the trend is expected to continue in the near future.

385 Similar plots but for the ice area are presented in Figure 12, and it is apparent that the  
386 variabilities are similar but the trends are more negative with the corresponding trends for the  
387 three cases being  $-4.01 \pm 0.18$ ,  $-4.38 \pm 0.19$  and  $-4.00 \pm 0.18$  %/decade. The more negative trend  
388 for ice area compared to those for ice extent is in part associated with a negative trend in the sea  
389 ice concentration during the period. Changes in ice concentration may be caused by changes in  
390 wind strength and wind patterns that in turn cause changes in the area affected by divergence. In  
391 the summer, it can also be caused by changes in the areal extent of meltponding which causes  
392 large errors in the estimate of ice concentration (Comiso and Kwok, 1995).

393 For completeness, regional trends in the ice extent are presented in Figure 13. While  
394 overall, the trend for the entire hemisphere is moderate at about  $-3.4 \pm 0.2$  %/decade there are  
395 regions where significantly higher negative trends are apparent. Among these regions are the  
396 Greenland Sea, the Kara/Barents Seas, the Okhotsk Sea, Baffin Bay/Labrador Sea, and the Gulf  
397 of St. Lawrence where the trends are -8.0, -7.2, -8.7, -8.6, and -10.7, respectively. In these  
398 regions, some cyclical patterns are also evident especially in the first 15 years of data. The only  
399 region that show positive trend is the Bering Sea which appears to be growing but at a negligible  
400 rate of  $1.7 \pm 2.0$  %/decade. This region is one of the few sea ice covered areas in the Arctic that  
401 has exhibited some cooling in the last few decades (Comiso, 2003).

402

#### 403 *4.2 The Southern Hemisphere*

404 Monthly extents and ice areas in the Southern Hemisphere, as derived from SMMR,  
405 SSM/I and AMSR data (Figure 14) show an even more seasonal ice cover than that of the  
406 Northern Hemisphere. Minimum ice extents and ice areas usually occurs in February while  
407 maximum ice extents and ice areas occurs in September. This means that the growth period takes  
408 a longer time than the melt period in the Southern Hemisphere (see also, Figure 6). The  
409 maximum and minimum extents and areas go through interannual fluctuations but they look  
410 relatively stable. However, it appears that since the winter of 2002, the maximum values have  
411 been increasing but at the same time, the minimum values have been decreasing. It would be  
412 interesting if the subsequent years would follow the same pattern and show some modulation in  
413 the ice cover.

414 The monthly ice extent anomalies are again presented for the three cases in the Southern  
415 Hemisphere (Figure 14) as in the Northern Hemisphere. It is apparent that there is large  
416 fluctuation in the monthly anomalies (of about  $2 \times 10^6 \text{ km}^2$ ) from 1978 through 1987 and then a  
417 much more moderate variation (of about  $1 \times 10^6 \text{ km}^2$ ) from 1987 to 1994 that is followed by a  
418 larger fluctuation from 1994 through 2006. The monthly extents (Figure 13) do not show large  
419 interannual changes during the 1987 to 1994 period and it is not known why the sea ice cover  
420 anomalies would go into such transition from high to low variability and then higher variability in  
421 the Southern Ocean. Using SMMR and SSM/I data only, the trend in the hemispheric ice extent  
422 is  $0.945 \pm 0.230 \text{ \%/decade}$  while with SMMR, SSM/I, and AMSR-E data, the trend is slightly  
423 lower at  $0.684 \pm 0.230 \text{ \%/decade}$ . The difference is again likely associated with differences in  
424 resolution as discussed earlier and if SMMR and SSM/I data are normalized to make them  
425 consistent with AMSR-E data, the trend is similar to the first, being  $0.94 \text{ \%/decade}$ . Again, in  
426 this way, AMSR-E data can be used in trend analysis in conjunction with historical data.

427 The corresponding monthly anomalies for ice area as presented in Figure 15 show the  
428 same variability as the ice extent. However, the trends are much more similar in all three cases  
429 the values being  $1.72 \pm 0.25$ ,  $1.77 \pm 0.26$  and  $1.72 \pm 0.25 \text{ \%/decade}$ . Again, the difference of the  
430 first two are minor because the contribution of additional pixels along the ice edge caused by  
431 differences in resolution does not affect the estimate of area as much as that of the ice extent.  
432 After the application of the normalization factors on the SMMR and SSM/I data, the trend in as  
433 indicated in Figure 15c of  $1.72 \text{ \%/decade}$  is virtually identical to that of Figure 15a.

434 Except for the summer, the sea ice cover around the Antarctic continent is contiguous and  
435 therefore, there is no natural boundary as in the Arctic region. For regional studies, we adapt the  
436 same sectors used in Zwally et al. (1983). The monthly anomalies for the entire hemisphere and  
437 for the different regions, as presented in Figure 16, have very similar variabilities with the  
438 possible exception of those in the Ross Sea Sector. The trends in ice extent for the various  
439 regions are all positive except that of the Belingshausen-Amundsen Seas Sector, which has been  
440 previously identified by Jacobs and Comiso (1997) as a climatologically anomalous region. The  
441 trend in this region is currently  $-5.7 \text{ \%/decade}$  but this is compensated by a positive trend of  $4.2$   
442  $\text{ \%/decade}$  in the Ross Sea. Some declines in the Ross Sea ice cover is apparent in recent years  
443 but they are more than compensated by increases at the Indian Ocean and the West Pacific Ocean.

444

445 **5. Sensitivity and Error Analysis**



446 To evaluate quantitatively how errors in the determination of the ice edge affects the  
447 estimates for the trends in ice extent and ice area we use the original values of SMMR and SSM/I  
448 and added a data element at the ice edge in the AMSR-E data. Since each data element has a grid  
449 size of about 25 by 25 km this means having an ice edge about 25 km further away. We also did  
450 the same for half a pixel and a quarter of a pixel to assess the effect of an ice edge being 12.5 and  
451 6.25 km further away as well. The results are presented in Figures 17 and 18, respectively, for  
452 the Northern Hemisphere and the Southern Hemisphere. In the Northern Hemisphere, the trend  
453 in extent ranges in value from -3.03%/decade for a bias of a full pixel to -3.99 % per decade for  
454 no bias. Comparing with our previous results, the bias at the ice edge is likely about 14 km. In  
455 the Southern Hemisphere, the trend in extent ranges from 2.16% per decade for a one pixel bias  
456 to 0.68% per decade for no bias. Comparing with our previous results, this translates a bias at the  
457 ice edge of about 6 km. The changes in trend for the areas are much smaller.

458

## 459 **6. Discussion and Conclusions**

460 The AMSR-E data provide opportunities to study the sea ice cover at higher accuracy and  
461 in greater spatial detail than ever before. The greater spectral range and higher resolution data set  
462 will enable more in depth studies of many mesoscale processes that occurs in polynyas,  
463 divergence areas and marginal ice zones. Comparative studies shows a good match of high  
464 resolution AMSR-E data with those of high resolution satellite data providing confidence that the  
465 interpretation of large scale as well as mesoscale features identified in the former are indeed  
466 accurate. With only about 5 years of good data available, however, the record length is too short  
467 for change studies. Change studies using AMSR-E data can thus be made effectively when it is  
468 combined with historical satellite data.

469 This study shows that during the overlap period from June 2002 to 2006 that the ice  
470 concentration maps derived from AMSR-E and SSM/I are virtually identical. The ice extents and  
471 ice areas estimated from the two sensors are also in very good agreement and both basically  
472 provide the same information about seasonal and interannual variability. The historical data  
473 therefore provide a reasonably accurate estimate of the trends in the ice cover. However, there  
474 are subtle differences, especially in the characterization of the Marginal Ice Zone and the ice  
475 edge. Because of higher resolution, AMSR-E is able to provide more precise locations and more  
476 accurate gradients in these regions that that provided by SSM/I. This difference is reflected in the  
477 estimates of ice extents with the latter providing slightly higher values on account of coarser

478 resolution. With proper normalization, however, the AMSR-E data can still be combined with  
479 the historical satellite data for more accurate determination of trends in ice extent. In the  
480 estimates of ice area, AMSR-E and SSM/I data provides almost identical values basically since  
481 the ice concentrations generally agree and the effect of additional low concentration ice at the ice  
482 edges detected by one but not the other is negligible in this estimate.

483 With the higher resolution and improved accuracy, AMSR-E data provide a good baseline  
484 for ice cover studies and to test the estimates in extent and area from other sensors. We show that  
485 because of coarser resolution, SSM/I data provides a location of the ice edge that is on the  
486 average about 6 to 12 km further away from the ice pack than AMSR-E data. Biases if  
487 uncorrected could also contribute to errors in the estimates of trends in extents of as much as  
488 0.62%/decade in the Arctic and 0.26%/decade in the Antarctic. The biases in ice area are less  
489 with the error in the trend of areas being at 0.30%/decade in the Arctic and 0.05%/decade in the  
490 Antarctic.

491 Using data from SMMR, SSM/I and AMSR-E and after correcting for the aforementioned  
492 bias, the results of our regression analysis for period from November 1978 to December 2006  
493 yielded trends in extent and area of sea ice in the Arctic region are  $-3.4 \pm 0.2$  and  $-4.0 \pm 0.2$  % per  
494 decade, respectively. The corresponding values for the Antarctic region are  $0.9 \pm 0.2$  and  $1.7 \pm$   
495  $0.3$  % per decade. These trends are basically the same as those derived using SMMR and SSM/I  
496 data only, but with better accuracy since AMSR-E provides more accurate data. With time, the  
497 data from AMSR-E and similar instruments will increase the reliability of the trend values.

498

499 **Acknowledgements:** The authors wish to express gratitude to the excellent programming  
500 support provided by Robert Gersten of Adnet, Inc. This research was supported by the  
501 Cryospheric Sciences Program of NASA Headquarters.

502

### 503 REFERENCES

504 Bjorgo, E. , O.M. Johannessen, and M.W. Miles, "Analysis of merged SSMR-SSM/I  
505 time series of Arctic and Antarctic sea ice parameters 1978-1995," *Geophys. Res.*  
506 *Lett.*, Vol. 24, pp. 413-416, 1997.

507 Cavalieri, D.J., P. Gloersen, W.J. Campbell, Determination of sea ice parameters with the  
508 Nimbus7 SMMR, *J. Geophys Res.*, 89, 5355-5369, 1984.

509 Cavalieri, D.J., P. Gloersen, C. Parkinson, J. Comiso, and H.J. Zwally, Observed hemispheric

510 asymmetry in global sea ice changes, *Science*, 278(7), 1104-1106,1997.

511 Cho, K., N. Sasaki, H. Shimoda, T. Sakata and F. Nishio, Evaluation and improvement of SSM/I  
512 sea ice concentration algorithms for the Sea of Okhotsk, *J. Remote Sensing of Japan*, 16(2),  
513 47-58, 1996.

514 Colony, R. and A. Thorndike, Sea ice motion as a drunkard's walk, *J. Geophys. Res*, 90, 965-974,  
515 1985.

516 Comiso, J. C., A rapidly declining Arctic perennial ice cover, *Geophys Res. Letts.*, 29(20), 1956,  
517 doi:10.1029/2002GL015650, 2002.

518 Comiso, J.C., Sea ice algorithm for AMSR-E, *Rivista Italiana di Telerilevamento (Italian Journal*  
519 *of Remote Sensing)*, 30/31, 119-130, 2004.

520 Comiso, J. C., D. J. Cavalieri, and T. Markus, Sea ice concentration, ice temperature, and  
521 snow depth, using AMSR-E data, *IEEE TGRS*, 41(2), 243-252, 2003.

522 Comiso, J.C., and K. Steffen, Studies of Antarctic sea ice concentrations from satellite  
523 data and their applications, *J. Geophys. Res.*, 106(C12), 31361-31385, 2001.

524 Comiso, J.C., J. Yang, S. Honjo, and R.A. Krishfield, The detection of change in the Arctic using  
525 satellite and buoy Data, *J. Geophys. Res.* 108(C12), 3384, doi:1029-2002jc001247, 2003.

526 Eicken, H., M.A. Lange, and G.S. Dieckmann, Spatial variability of sea-ice properties in the  
527 northwestern Weddell Sea, *J. Geophys. Res.*, 96, 10,603-10,615, 1991

528 Gloersen P., W. Campbell, D. Cavalieri, J. Comiso, C. Parkinson, H.J. Zwally, Arctic and  
529 Antarctic Sea Ice, 1978-1987: Satellite Passive Microwave Observations and  
530 Analysis, *NASA Spec. Publ.* 511, 1992.

531 Grenfell, T.C. 1992.Surface-based passive microwave studies of multiyear ice. *J. Geophys. Res.*,  
532 97(C3), 3485-3501.

533 Kumerow, C, On the accuracy of the Eddington approximation for radiative transfer in  
534 the microwave frequencies," *J. Geophys. Res*, Vol. 98, pp. 2757- 2765, 1993.

535 Matzler, C., R. O. Ramseier, and E. Svendsen, "Polarization effects in sea ice  
536 signatures," *IEEE J. Oceanic Engineering*, Vol. OE-9, pp. 333-338, 1984.

537 Overland, J.E., The Arctic climate paradox: The recent decrease of the Arctic Oscillation,  
538 *Geophys. Res. Letters*, 32, L06701, doi:10.1029/2004GL021752, 2005.

539 Parkinson, C.L., D.J Cavalieri, P. Gloersen, H.J. Zwally, and J.C. Comiso, Arctic sea ice  
540 extents, areas, and trends, 1978-1996, *J. Geophys. Res.*, 104(C9), 20837-20856, 1999.

541 Parkinson, C. L., J. C. Comiso, H. J. Zwally, D. J. Cavalieri, P. Gloersen, and W. J. Campbell,

542 Arctic Sea Ice 1973-1976 from Satellite Passive Microwave Observations, *NASA Spec. Publ.*  
543 489, 1987.

544 Serreze, M.C., and Co-authors, Observational evidence of recent change in the northern high-  
545 latitude environment, *Climatic Change*, 46, 159-207, 2000.

546 Steffen, K., D. J. Cavalieri, J. C. Comiso, K. St. Germain, P. Gloersen, J. Key, and I. Rubinstein,  
547 "The estimation of geophysical parameters using Passive Microwave Algorithms," Chapter 10,  
548 *Microwave Remote Sensing of Sea Ice*, (ed. by Frank Carsey), American Geophysical Union,  
549 Washington, D.C., 201-231, 1992.

550 Stroeve, J.C., M.C., Serreze, F. Fetterer, T. Arbetter, M. Meier, J. Maslanik and K. Knowles,  
551 Tracking the Arctic's shrinking ice cover: Another extreme September minimum in 2004,  
552 *Geophys. Res. Lett.* 32, doi:10.1029/2004GL021810, 2004.

553 Svendsen, E., C. Matzler, T.C. Grönfäll, "A model for retrieving total sea ice  
554 concentration from a spaceborne dual-polarized passive microwave instrument  
555 operating near 90 GHz," *Int. J. Rem. Sens.*, Vol. 8, pp. 1479-1487, 1987.

556 Swift, C.T., L.S. Fedor, and R.O. Ramseier, An algorithm to measure sea ice concentration with  
557 microwave radiometers, *J. Geophys. Res.*, 90(C1), 1087-1099, 1985.

558 Tucker, W.B., D.K. Perovich, and A.J. Gow, "Physical properties of sea ice relevant to remote  
559 sensing," Chapter 2, *Microwave Remote Sensing of Sea Ice*, (ed. by Frank Carsey), American  
560 Geophysical Union, Washington, D.C., 9-28, 1992.

561 Vant, M.R., R.B. Gray, R.O. Ramseier, and V. Makios. 1974. Dielectric properties of fresh and  
562 sea ice at 10 and 35 GHz, *J. Applied Physics*, 45(11), 4712-4717.

563 Weeks, W.F., and S. F. Ackley, The growth, structure and properties of sea ice, *The Geophysics*  
564 *of Sea Ice*, edited by N. Unterstiener, pp. 9-164, *NATO ASI Ser.B*, vol. 146, Plenum, New  
565 York, 1986.

566 Worby, A. P., and J. C. Comiso, Studies of Antarctic sea ice edge and ice extent from satellite  
567 and ship observations, *Remote Sensing of the Environment*, 92(1), 98-111, 2004.

568 Zwally, H.J., J.C. Comiso, C. Parkinson, D. Cavalieri, P. Gloersen, Variability of the  
569 Antarctic sea ice cover, *J. Geophys. Res.* 107(C5), 1029-1047, 2002.

570 Zwally, H. J., J. C. Comiso, C. L. Parkinson, W. J. Campbell, F. D. Carsey, and P. Gloersen,  
571 Antarctic Sea Ice 1973-1976 from Satellite Passive Microwave Observations, *NASA Spec.*  
572 *Publ.* 459, 1983.

573

574

575

576 **Figure Captions:**

577 Figure 1. Location map for (a) the Northern Hemisphere; and (b) the Southern Hemisphere. The  
578 two shades of gray correspond to the climatological average of the location of the ice cover  
579 during minimum and maximum extent.

580 Figure 2. Daily ice concentration maps during winter in the (a) Northern Hemisphere using  
581 AMSR-E data; (b) Northern Hemisphere using SSM/I data; (c) Southern Hemisphere using  
582 AMSR-E data; and (d) Southern Hemisphere using SSM/I data.

583 Figure 3. Scatter plots of TB(V19, V) versus TB(22, V) - TB(19, V) for (a) SSM/I and (b)  
584 AMSR-E data. Also, scatter plots of TB(19,V) versus TB(37,V) for (c) SSM/I and (d) AMSR-E  
585 data.

586 Figure 4. Transects along the ice edges of brightness temperatures using AMSR-E (a) vertically  
587 polarized and (b) horizontally polarized data and (c) comparison of ice edges as inferred from ice  
588 concentration values of AMSR-E and SSM/I.

589 Figure 5. Ice concentrations along the ice edge in the Barents Sea at (a) 35 °E and (b) 45 °E.

590 Figure 6. Daily ice extents (a &b), ice area (c & d), and ice concentration (e & f) during a period  
591 of SSM/I and AMSR-E overlap (2005) in the Northern and Southern Hemispheres

592 Figure 7. Daily ice extent (a &b), ice area (c & d), and ice concentration (e & f) during a period  
593 of SSM/I (F11) and SSM1(F13) overlap (May to September 1995) in the Northern and Southern  
594 Hemispheres.

595 Figure 8. Daily extent (a &b), ice area (c & d), and ice concentration (e & f) during a period of  
596 SMMR and SSM/I overlap in the Northern and Southern Hemispheres (July to August 1987).

597 Figure 9. Monthly extent and area from 1978 to 2006 in the Northern Hemisphere using SMMR,  
598 SSM/I and AMSR-E data time series data.

599 Figure 10. Monthly anomaly and trend in extents from 1978 to the present in the Northern  
600 Hemisphere using (a) original SMMR and SSM/I data; (b) original SMMR, SSM/I (up to May  
601 2002) and AMSR-E data (June 2002 to 2006); and (c) normalized SMMR and SSM/I data and  
602 original AMSR-E data.

603 Figure 11. Monthly anomaly and trend in ice area from 1978 to the present in the Northern  
604 Hemisphere using (a) original SMMR and SSM/I data; (b) original SMMR, SSM/I (up to May

605 2002) and AMSR-E (June 2002 to 2006) data; and (c) normalized SMMR and SSM/I data and  
606 original AMSR-E data.

607 Figure 12. Monthly anomalies of ice extent in the (a) Northern Hemisphere and in the following  
608 regional sectors: (b) Arctic Ocean; (c) Greenland Sea; (d) Kara/Barents Sea, (e) Bering Sea; (f)  
609 Okhotsk/Japan Seas; (g) Canadian Archipelago; (h) Baffin Bay/Labrador Sea; (i) Hudson Bay;  
610 and (j) Gulf of St. Lawrence.

611 Figure 13. Monthly extent and area from 1978 to the present in the Southern Hemisphere using  
612 SMMR SSM/I and AMSR-E data

613 Figure 14. Monthly anomaly and trend in extents from 1978 to the present in the Southern  
614 Hemisphere using (a) original SMMR and SSM/I data; (b) original SMMR, SSM/I (up to May  
615 2002) and AMSR-E (from June 2002 to 2006) data; and (c) normalized SMMR and SSM/I data  
616 and original AMSR-E data.

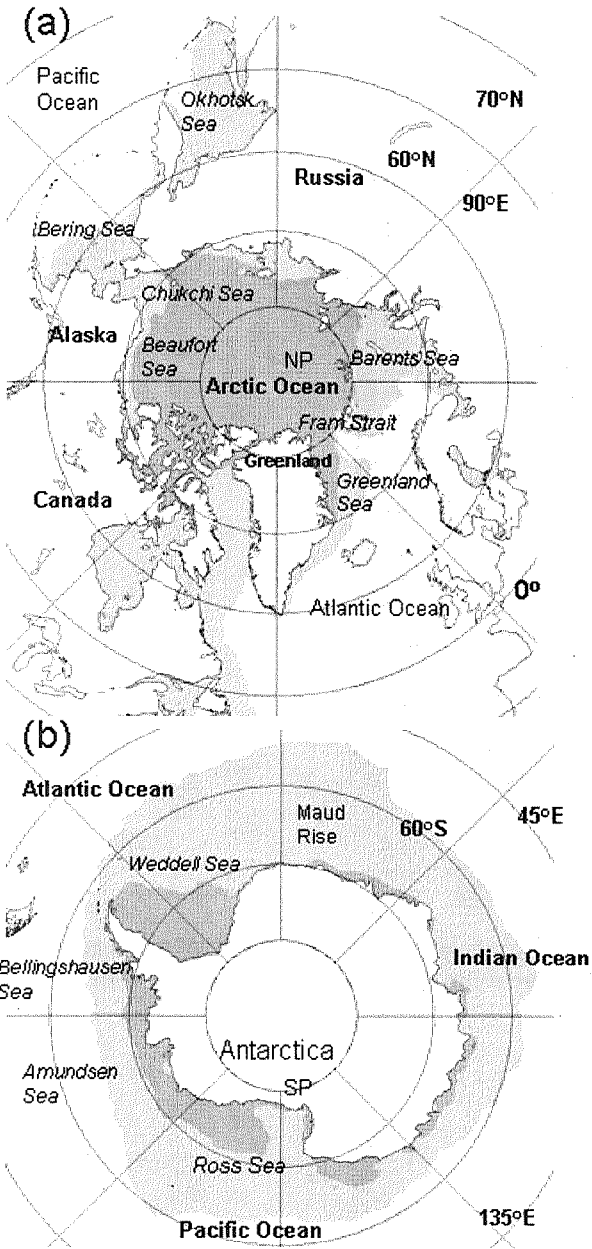
617 Figure 15. Monthly anomaly and trend in ice area from 1978 to the present in the Southern  
618 Hemisphere using (a) original SMMR and SSM/I data; (b) original SMMR, SSM/I and AMSR-E  
619 data; and (c) normalized SMMR and SSM/I data and original AMSR-E data.

620 Figure 16. Monthly anomalies of ice extent in the (a) Southern Hemisphere and in the following  
621 regional sectors: (b) Weddell Sea; (c) Indian Ocean; (d) West Pacific Ocean; (e) Ross Sea; (f)  
622 Bellingshausen/Amundsen Seas.

623 Figure 17. Sensitivity of trends to (a) ice extent and (b) ice area with adjustments of AMSR-E  
624 data by making the ice edge 6.25, 12.5, and 25 km further away from the ice pack in the Northern  
625 Hemisphere during an entire ice season.

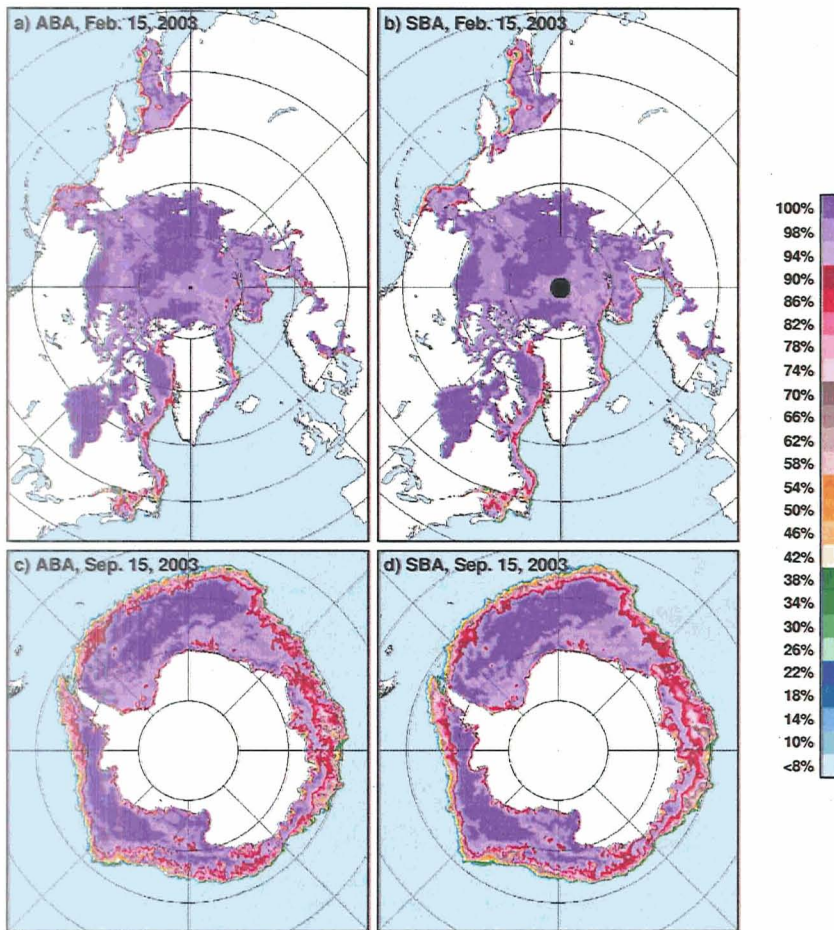
626 Figure 18. Sensitivity of trends to (a) ice extent and (b) ice area with adjustments of AMSR-E  
627 data by making the ice edge 6.25, 12.5, and 25 km further away from the ice pack in the Southern  
628 Hemisphere during an entire ice season.

629



630  
631  
632

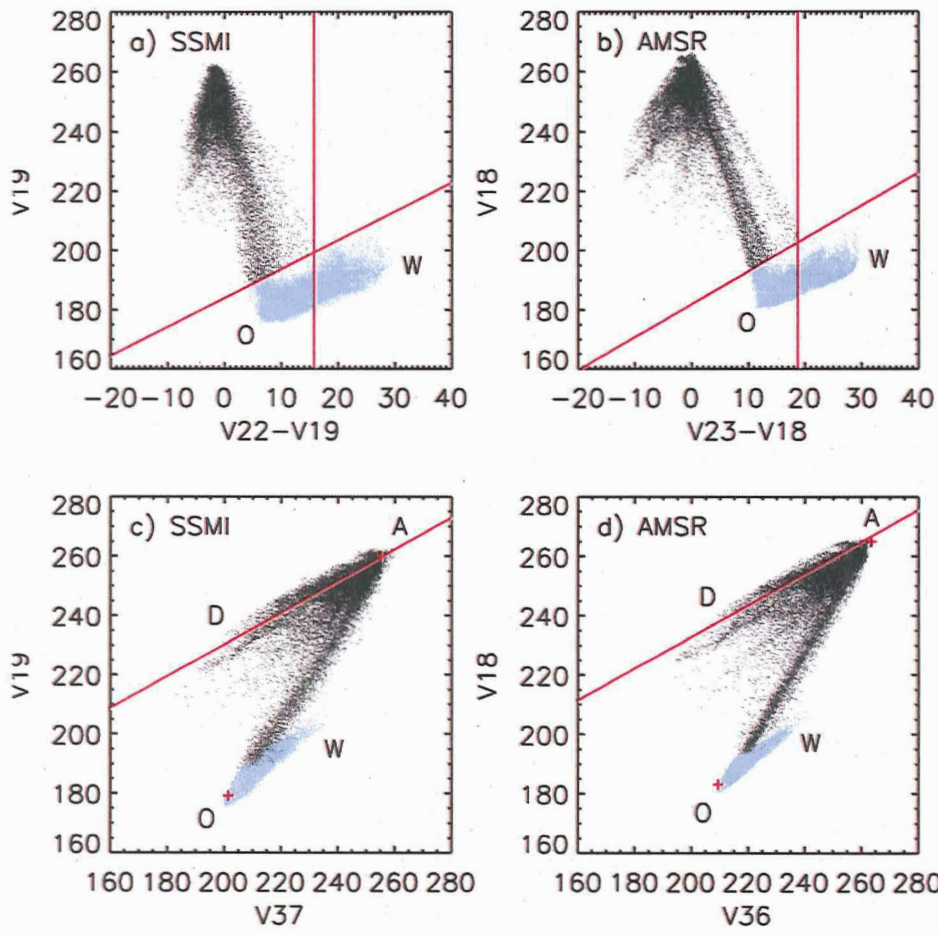
Figure 1. Location map for (a) the Northern Hemisphere; and (b) the Southern Hemisphere. The two shades of gray correspond to the climatological average of the location of the ice cover during minimum and maximum extent.



633  
 634  
 635  
 636  
 637  
 638  
 639  
 640

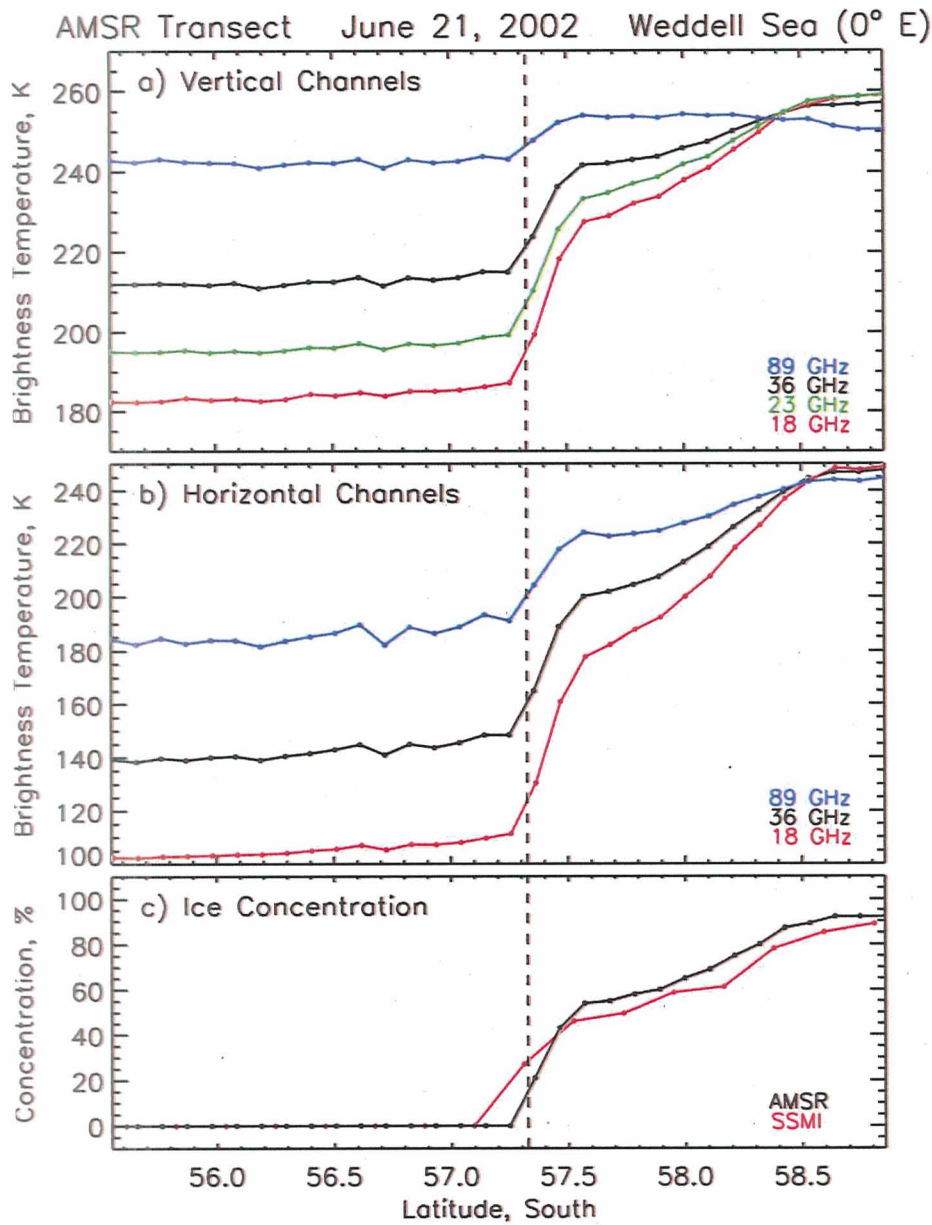
Figure 2. Daily ice concentration maps during winter in the (a) Northern Hemisphere using AMSR-E data; (b) Northern Hemisphere using SSM/I data; (c) Southern Hemisphere using AMSR-E data; and (d) Southern Hemisphere using SSM/I data.





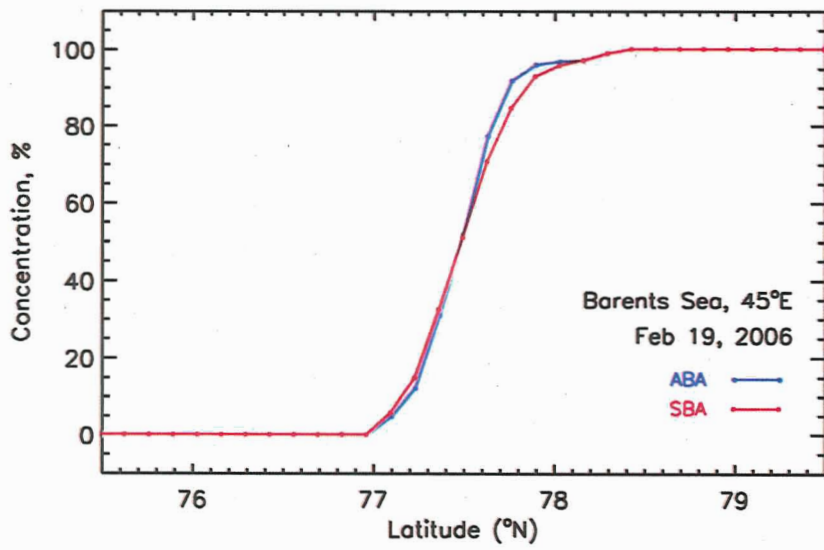
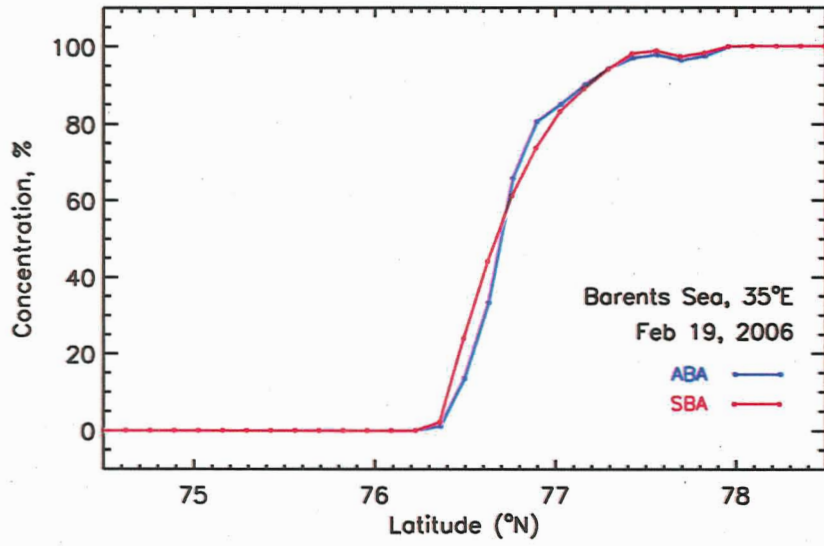
641  
 642  
 643  
 644  
 645  
 646

Figure 3. Scatter plots of TB(V19, V) versus TB(22, V) - TB(19, V) for (a) SSM/I and (b) AMSR-E data. Also, scatter plots of TB(19, V) versus TB(37, V) for (c) SSM/I and (d) AMSR-E data.

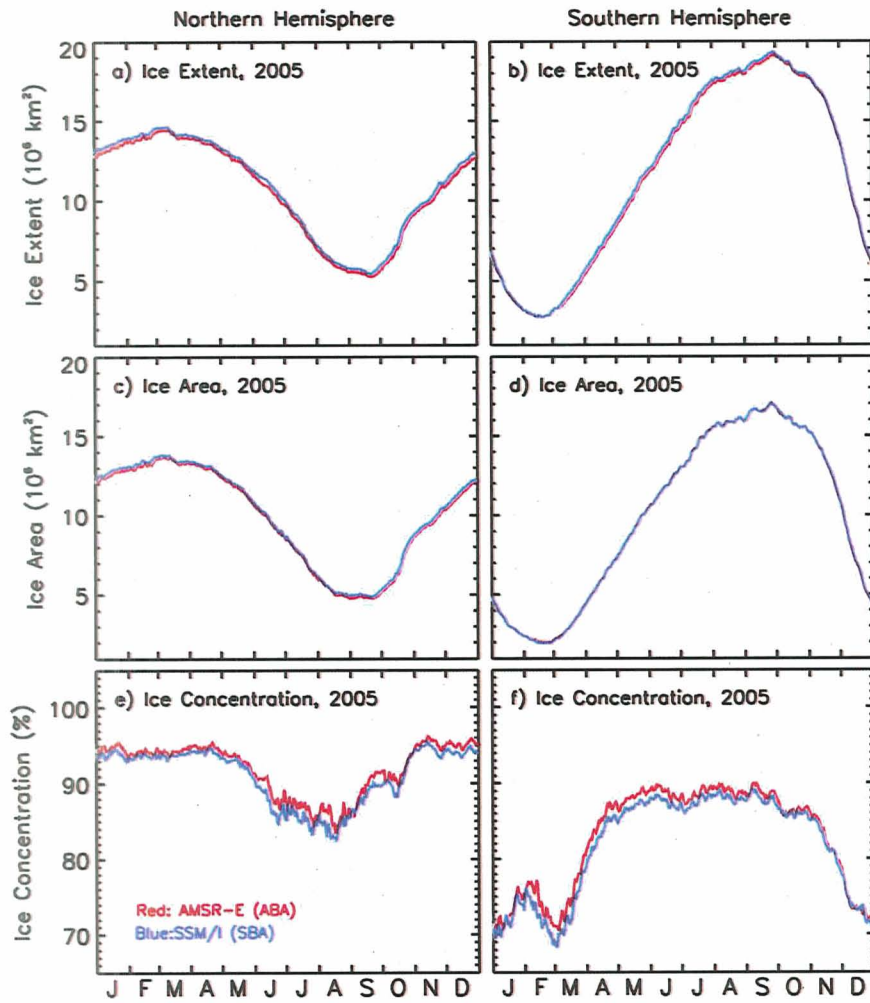


647  
648  
649  
650  
651

Figure 4. Transects along the ice edge of brightness temperatures using AMSR-E (a) vertically polarized and (b) horizontally polarized data and (c) comparison of ice edges as inferred from ice concentration values of AMSR-E and SSM/I.

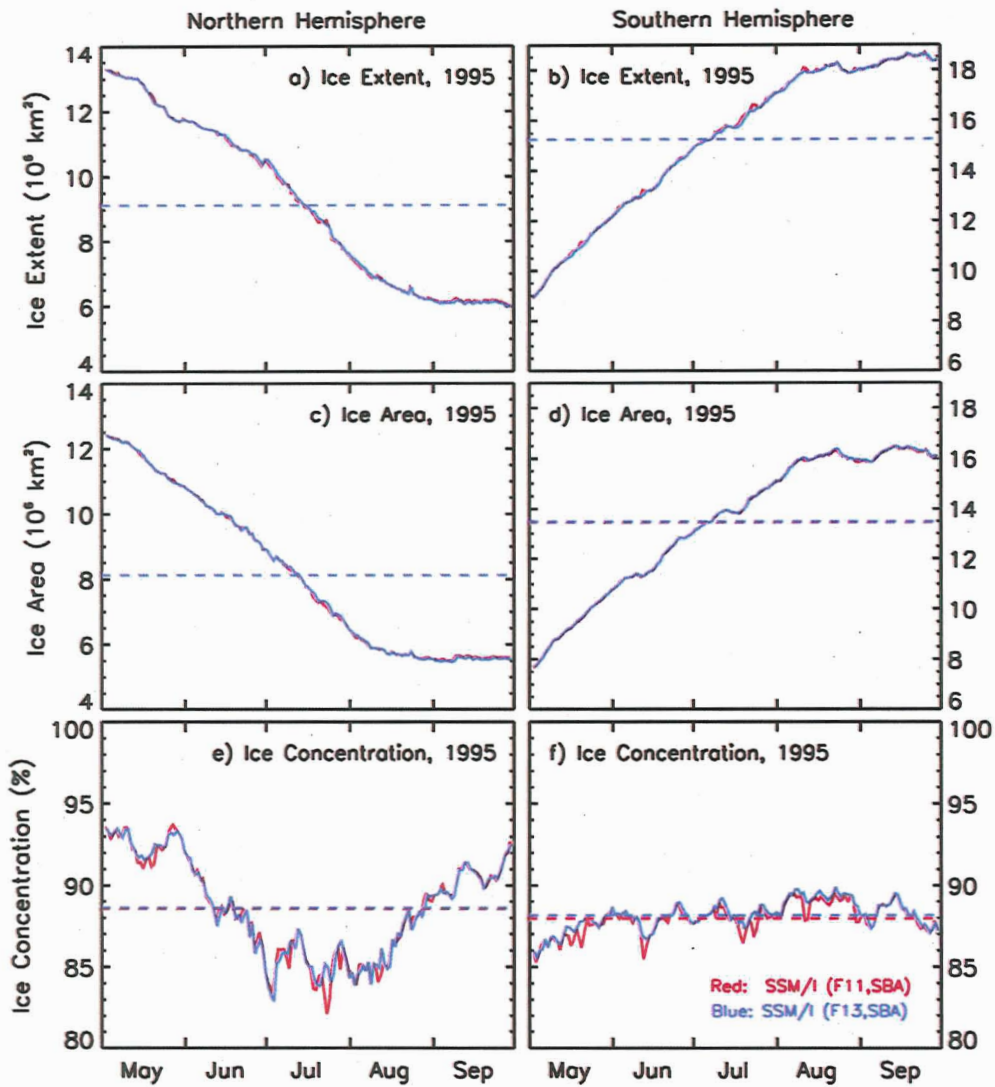


652  
653 Figure 5. Ice concentrations along the ice edge in the Barents Sea at (a) 35 °E and (b) 45 °E.  
654



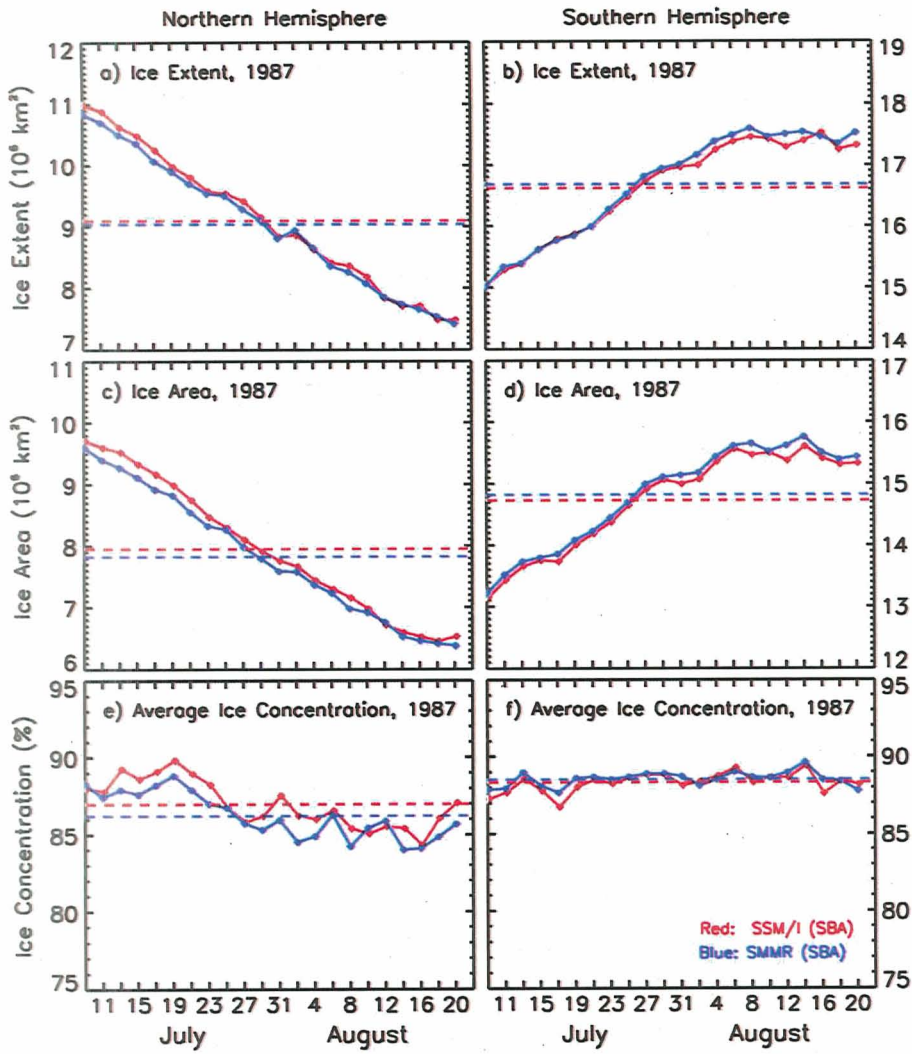
655  
656  
657

Figure 6. Daily ice extents (a & b), ice area (c & d), and ice concentration (e & f) during a period of SSM/I and AMSR-E overlap (2005) in the Northern and Southern Hemispheres



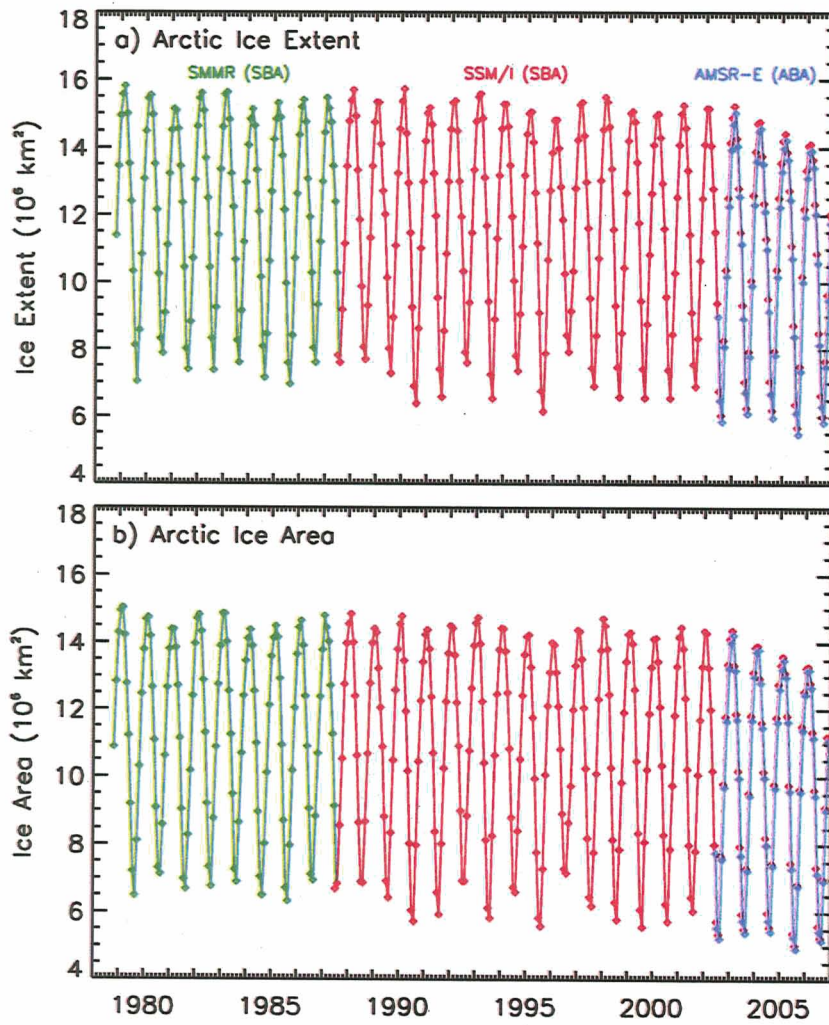
658  
 659  
 660  
 661  
 662  
 663

Figure 7. Daily ice extent (a & b), ice area (c & d), and ice concentration (e & f) during a period of SSM/I (F11) and SSM/I (F13) overlap (May to September 1995) in the Northern and Southern Hemispheres.



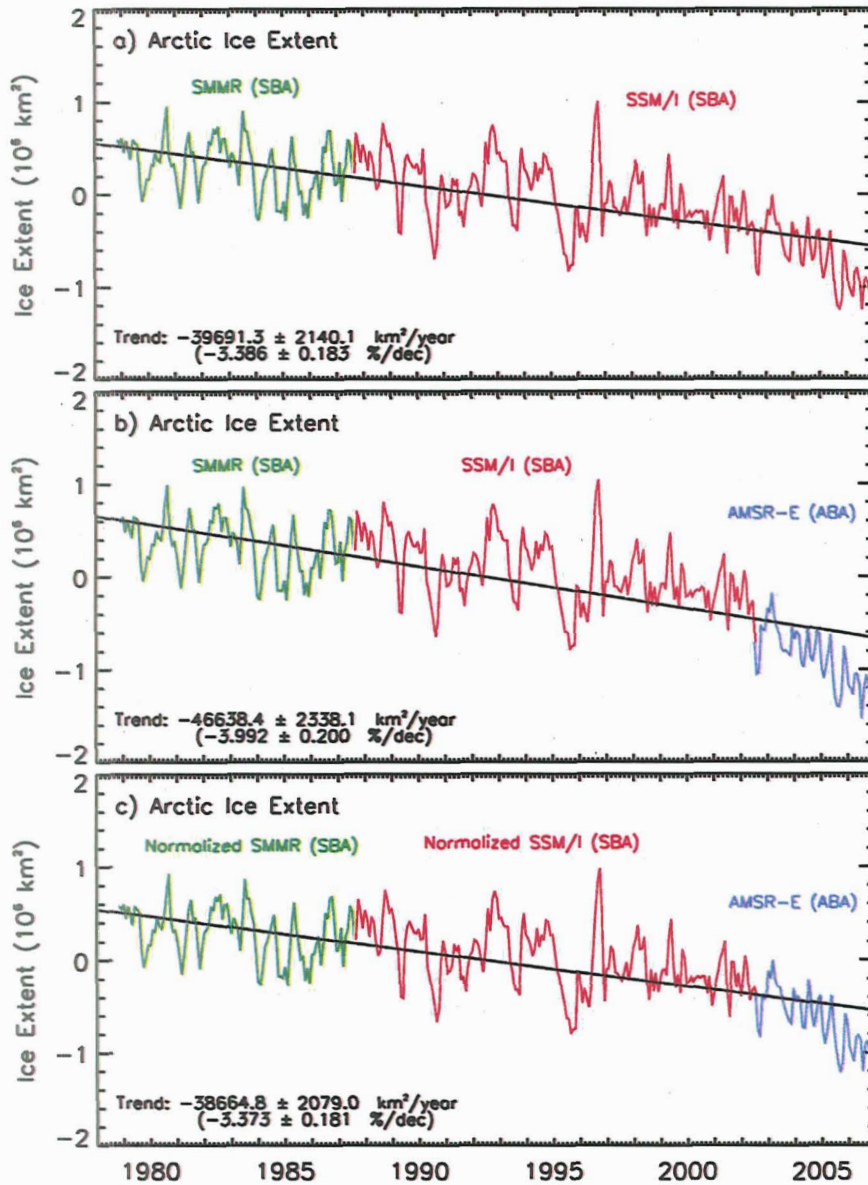
664  
 665  
 666  
 667  
 668  
 669  
 670  
 671

Figure 8. Daily extent (a & b), ice area (c & d), and ice concentration (e & f) during a period of SMMR and SSM/I overlap in the Northern and Southern Hemispheres (July to August 1987).



672  
 673  
 674  
 675  
 676

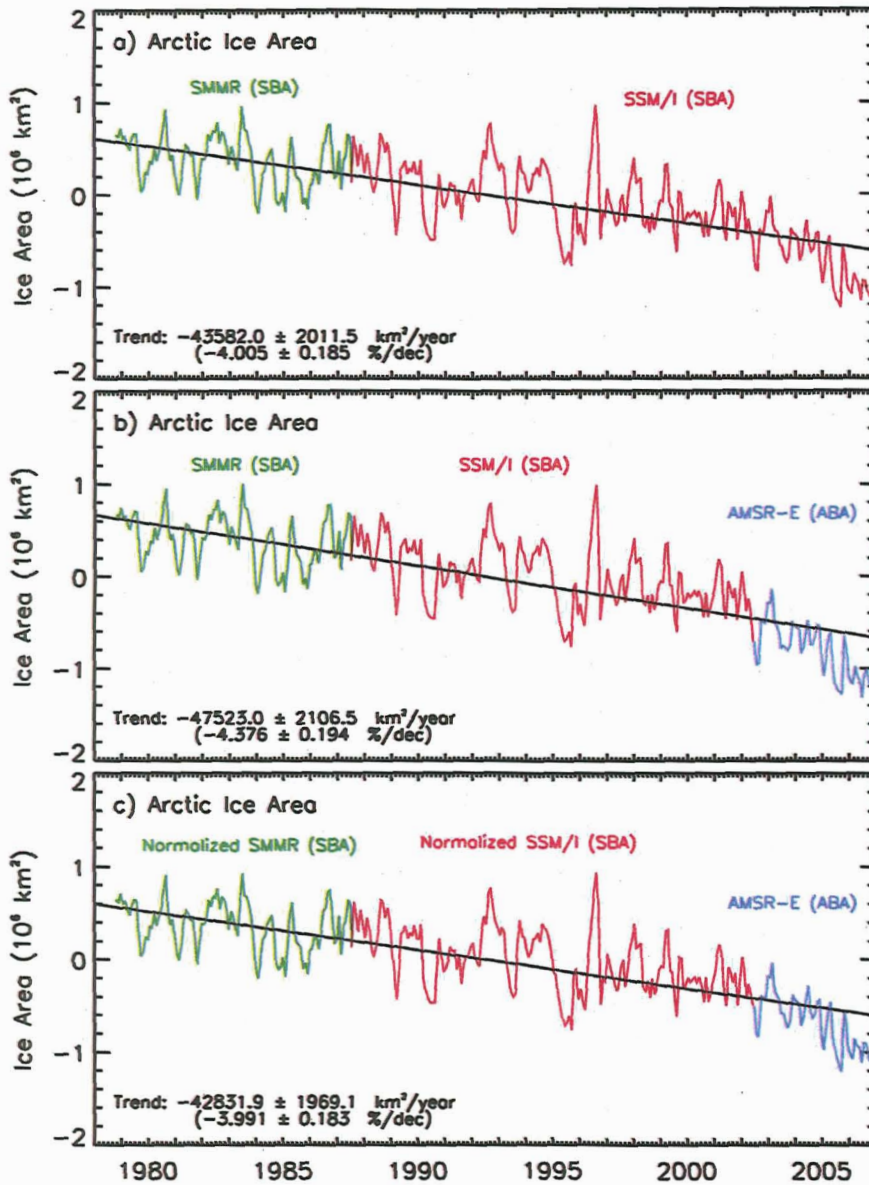
Figure 9. Monthly extent and area from 1978 to 2006 in the Northern Hemisphere using SMMR, SSM/I and AMSR-E data time series data.



677  
 678  
 679  
 680  
 681  
 682

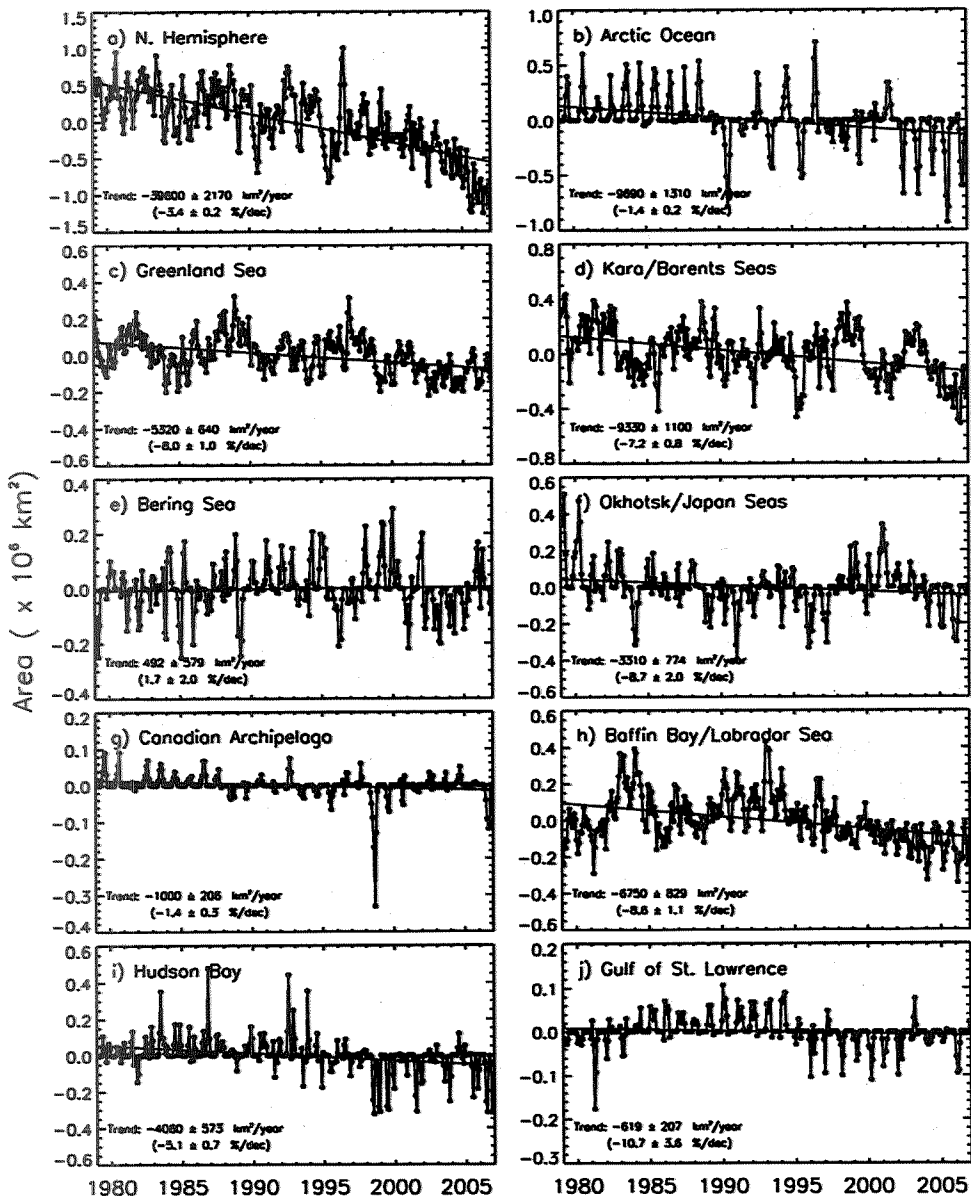
Figure 10. Monthly anomaly and trend in extents from 1978 to the present in the Northern Hemisphere using (a) original SMMR and SSM/I data; (b) original SMMR, SSM/I (up to May 2002) and AMSR-E data (June 2002 to 2006); and (c) normalized SMMR and SSM/I data and original AMSR-E data.





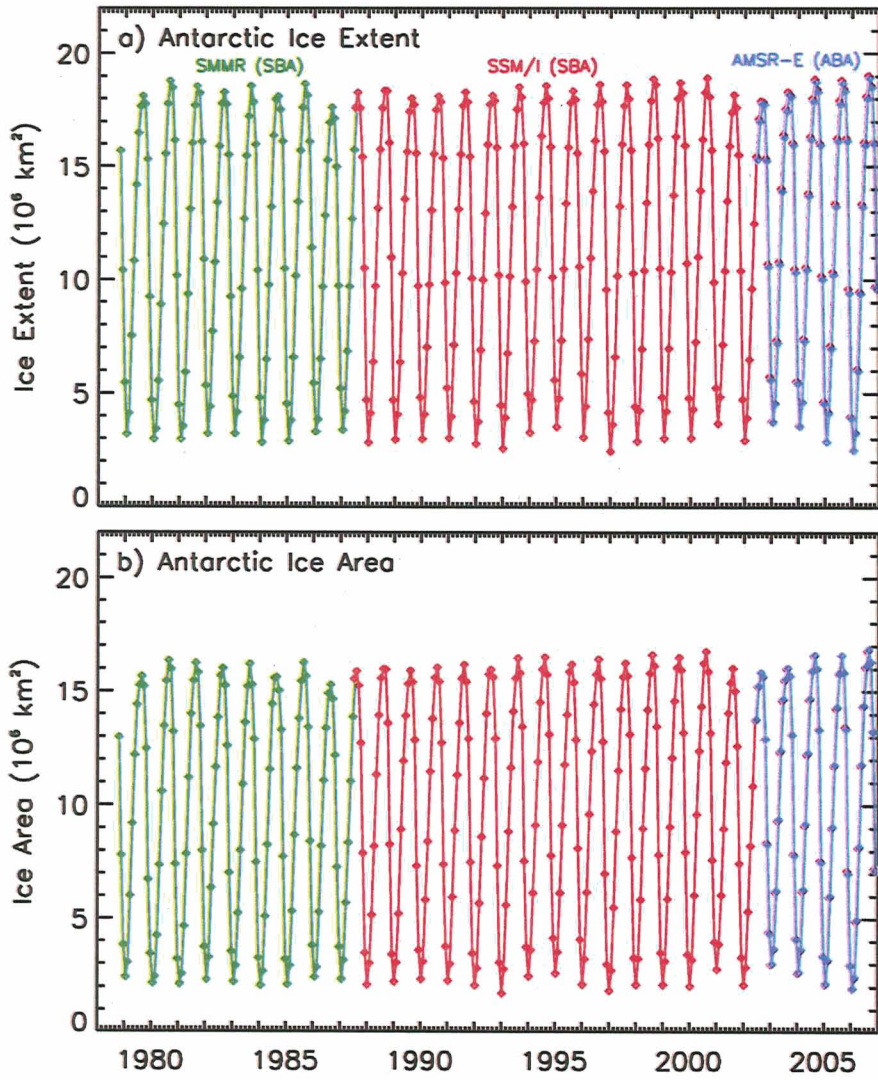
683  
 684  
 685  
 686  
 687  
 688  
 689

Figure 11. Monthly anomaly and trend in ice area from 1978 to the present in the Northern Hemisphere using (a) original SMMR and SSM/I data; (b) original SMMR, SSM/I (up to May 2002) and AMSR-E (June 2002 to 2006) data; and (c) normalized SMMR and SSM/I data and original AMSR-E data.



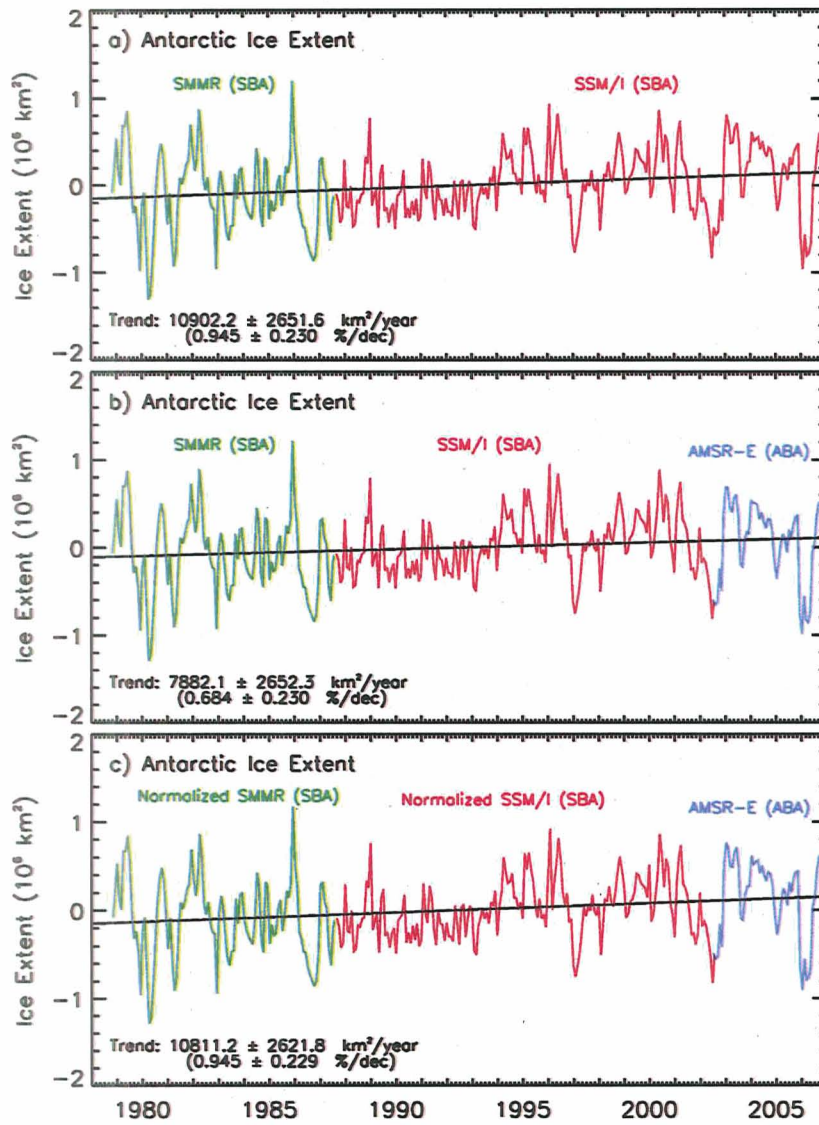
690  
691  
692  
693  
694

Figure 12. Monthly anomalies of ice extent in the (a) Northern Hemisphere and in the following regional sectors: (b) Arctic Ocean; (c) Greenland Sea; (d) Kara/Barents Sea, (e) Bering Sea; (f) Okhotsk/Japan Seas; (g) Canadian Archipelago; (h) Baffin Bay/Labrador Sea; (i) Hudson Bay; and (j) Gulf of St. Lawrence.



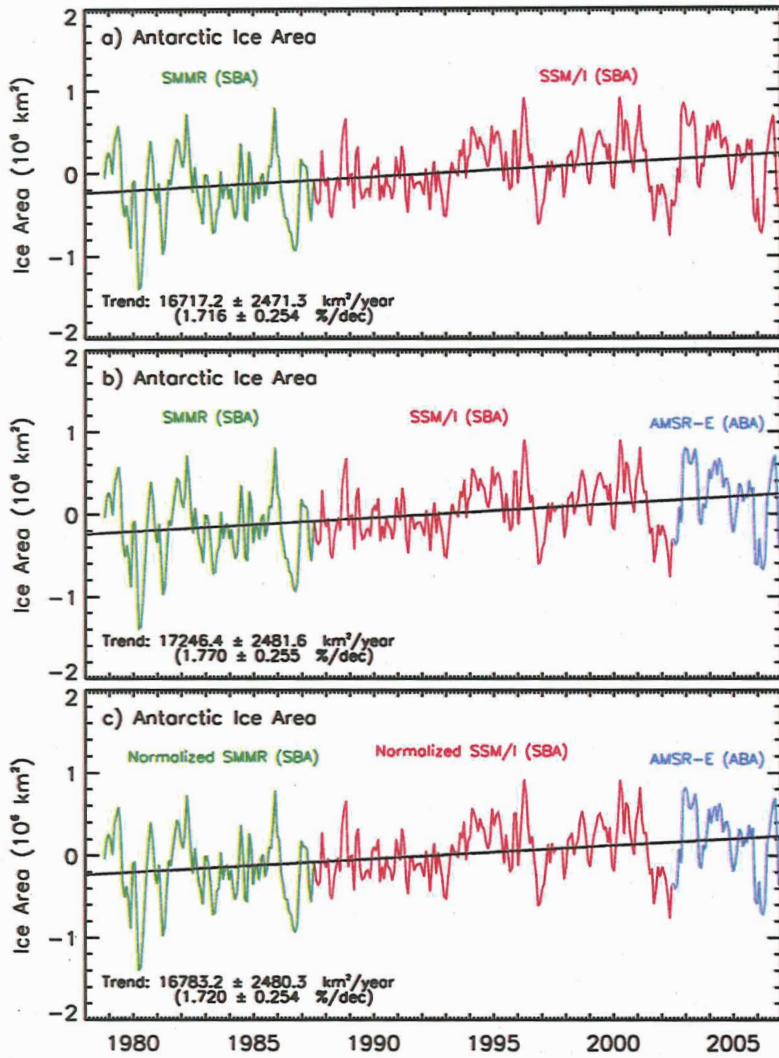
695  
 696  
 697  
 698  
 699

Figure 13. Monthly extent and area from 1978 to the present in the Southern Hemisphere using SMMR SSM/I and AMSR-E data



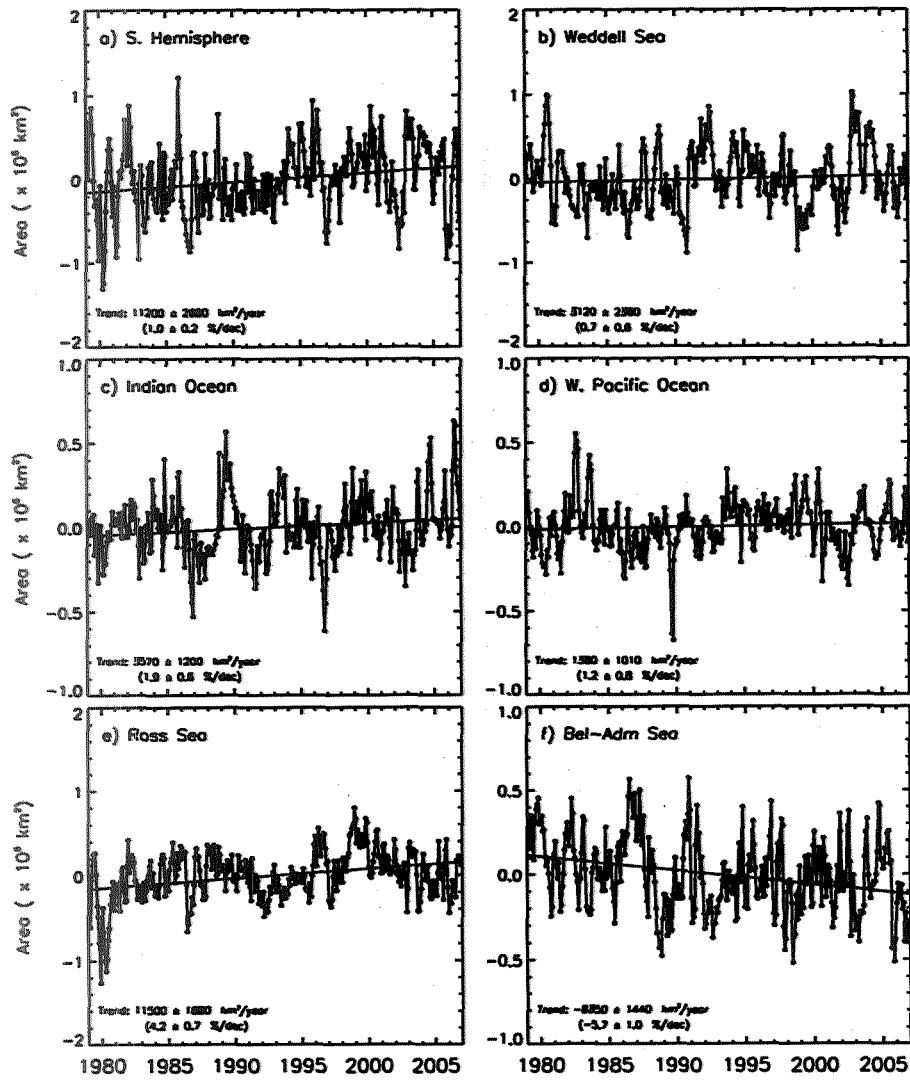
700  
 701  
 702  
 703  
 704  
 705

Figure 14. Monthly anomaly and trend in extents from 1978 to the present in the Southern Hemisphere using (a) original SMMR and SSM/I data; (b) original SMMR, SSM/I (up to May 2002) and AMSR-E (from June 2002 to 2006) data; and (c) normalized SMMR and SSM/I data and original AMSR-E data.



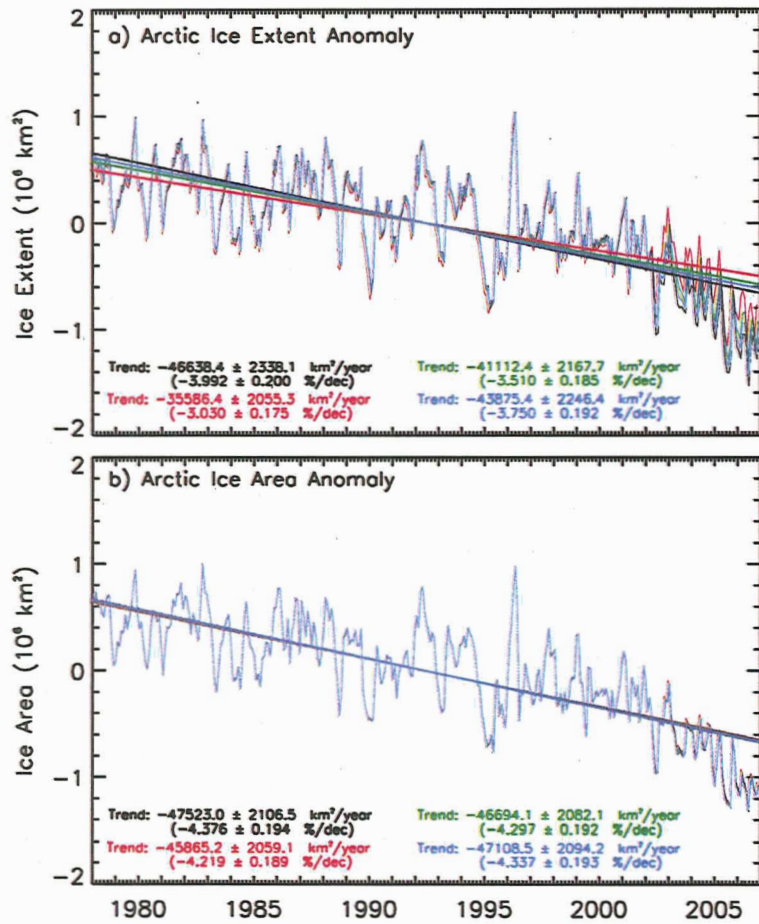
706  
 707  
 708  
 709  
 710  
 711  
 712

Figure 15. Monthly anomaly and trend in ice area from 1978 to the present in the Southern Hemisphere using (a) original SMMR and SSM/I data; (b) original SMMR, SSM/I and AMSR-E data; and (c) normalized SMMR and SSM/I data and original AMSR-E data.



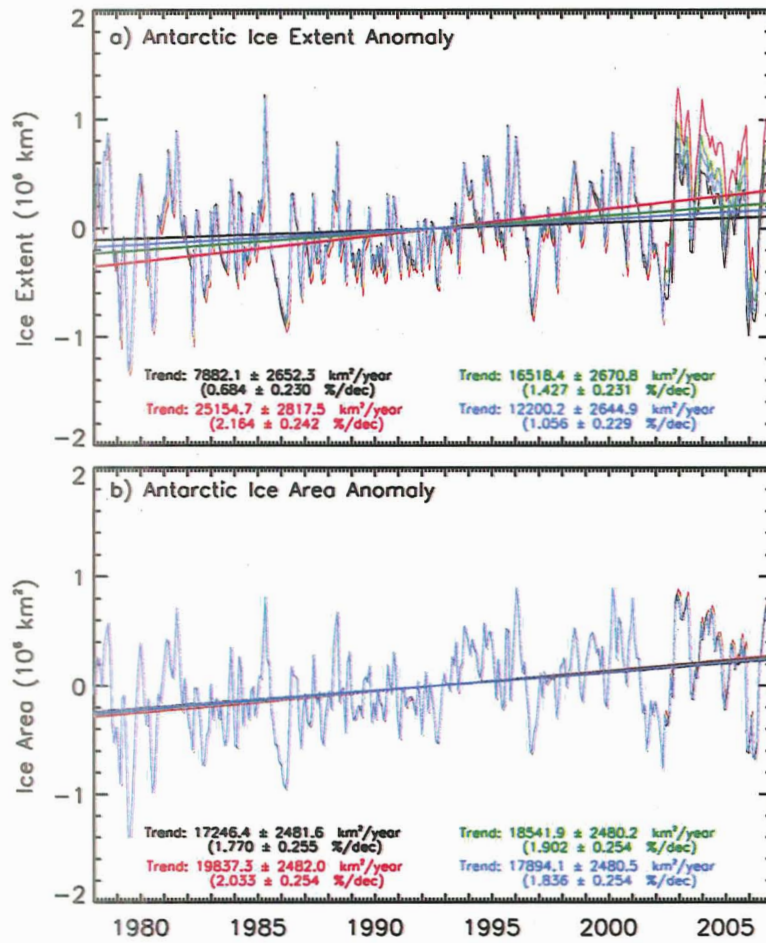
713  
714  
715  
716  
717  
718

Figure 16. Monthly anomalies of ice extent in the (a) Southern Hemisphere and in the following regional sectors: (b) Weddell Sea; (c) Indian Ocean; (d) West Pacific Ocean; (e) Ross Sea; (f) Bellingshausen/Amundsen Seas.



719  
720  
721  
722  
723  
724

Figure 17. Sensitivity of trends to (a) ice extent and (b) ice area with adjustments of AMSR-E data by making the ice edge 6.25, 12.5, and 25 km further away from the ice pack in the Northern Hemisphere during an entire ice season.



725  
 726  
 727  
 728  
 729  
 730  
 731

Figure 18. Sensitivity of trends to (a) ice extent and (b) ice area with adjustments of AMSR-E data by making the ice edge 6.25, 12.5, and 25 km further away from the ice pack in the Southern Hemisphere during an entire ice season.